Rapports internes du LaMSID

S. ANDRIEUX – T. BARANGER*

An energy error-based method for the resolution of the Cauchy problem in 3D linear elasticity

RI-B3-N°008 Juillet 2007

*LaMCOS INSA Lyon CNRS UMR 5259

Laboratoire de Mécanique des Structures Industrielles Durables
UMR EDF-CNRS 2832
EDF R&D
1, Avenue du Général de Gaulle - 92141 CLAMART CEDEX FRANCE

An energy error-based method for the resolution of the Cauchy problem in 3D linear elasticity

Stéphane Andrieux [a*] and Thouraya N. Baranger [b]

[a] *Mechanics of Durable Industrial Structures Laboratory, UMR CNRS-EDF 2832, Clamart, France*

[b] *Laboratoire de Mécanique des Contacts et des Structures*
LaMCoS, INSA-Lyon, CNRS UMR5259, F69621, France ;
Université de Lyon, Lyon, F-69003, France; Université Lyon 1, Villeurbanne, F-69622, France

Abstract

A new method is described for the problem of expanding known displacement fields at the boundary of a solid together with the surface tractions on it, towards the solid interior up to the inaccessible part of the boundary. The solid is supposedly linearly elastic with known elastic moduli (but not necessarily homogeneous nor isotropic). The problem is the Cauchy problem for the Lamé Operator. A new form of this Cauchy problem suited for applications associated with surface tangential fields' measurements is also stated and studied. The method is based on the splitting of the elastic fields into two separate solutions of well-posed problems; the gap between these fields is subsequently minimised with respect to the unknown boundary data in order to produce the desired expanded elastic fields. The gap used here is an energy error associated with the elastic energy of the system. Various 3D applications are given, including non-linear boundary conditions on the unreachable boundary.

Keywords: Cauchy problem, Boundary condition identification, Elasticity, Indentation, Contact, Inverse problem.

[*] Corresponding author. Tel.: (33) +1-47-65-15-80.
E-mail address : Stephane.Andrieux@edf.fr (S. Andrieux).

1 Introduction

The recent and rapid development of full-surface field imaging (Sutton *et al*., 1986) gives a new topicality to the classical Cauchy problem of expanding a field, whose dual quantity field is known on a part of a solid's boundary, towards the interior of the solid. The problem can also be seen as a data completion problem, a search for information lacking on a part of the solid's boundary when overspecified data are available on another part of the boundary. Various applications can be identified, including inverse problem applications (identification of unknown, possibly nonlinear, boundary conditions; geometrical inverse problems; identification of material parameters in a geometrically known inclusion embedded in an elastic solid; estimation of contact zones; etc.), damage detection or distributed material parameters identification (the data completion being the first step of the identification procedure). However, direct imaging applications could also complement 3D tomography imaging techniques, which give geometrical information with quantitative estimates of stress fields.

In this paper, a numerically efficient and physically well-grounded method is described and some preliminary applications with numerically produced *measurements* are given. The method is quite general and applications have also been studied for temperature field expansion and boundary condition recoveries (Andrieux et al., 2006). Here, the equations of linear elasticity are studied and the field expansion concerns the displacement field inside the solids, provided that displacement field is known on a part of the boundary. Also studied is a new kind of Cauchy problem which deals only with tangential surface displacement data in order to tackle the rapid development of image correlation tools that deliver only tangential information on surface displacement or strain fields.

The Cauchy problem for elliptic operators has been extensively studied for the Laplace operator, but more recent interest in the Lamé operator has appeared in linearized elasticity. Various methods have been proposed using front propagation methods (Bui, 1994), moment methods (Hon & Wei, 2001), fixed point algorithms (Koslov et al., 1999, Marin & Lesnic, 2004), evanescent regularization (Cimetiere et al. 2001, Delvare & Hanus 2005), quasi-reversibility approaches (Bourgeois, 2005), conformal mapping and Tikhonov regularization (Bernstsson & Elden, 2001), boundary elements methods (Marin & Lesnic, 2002) or direct approaches based on matrix rearrangement (Brian et al., 2004). Very few authors deal with this 3D problem because of the complexity of extending their method to 3D situations or because of computational costs. A large amount of work addresses only homogeneous and isotropic media. The present formulation aims simultaneously at more generality in order to deal with more realistic applications, and more computational efficiency in order to deal with large 3D situations.

Some ideas grounding the method can also be found in the approach of Brown *et al*. (2005), where a variational formulation of the Cauchy Problem for the Laplace operator is proposed. In his paper, the central role of the energy of the problem is recognized: it enables generalized variational approaches, leads to good convexity properties of the objective functional, and lastly results in a computationally efficient expression of the functional and of the adjoint problems used for computation of its gradients. The energy functional, or more exactly the error in the constitutive equation functionals which share some aspects with the present method, has been used for mesh refinement criteria (Ladeveze *et al*, 1994) and for parameter identification problems (Allix *et al*., 2003, Hadj-Sassi *et al*, 2006); however, up to now, this error has not been used in Cauchy or data completion problems.

The paper is organized as follows. In the upcoming section, the Cauchy problem and the so-called Incomplete Cauchy problem for the Lamé operator are defined, and some existing results on the uniqueness of the solution of the first one are reviewed while some insights into the uniqueness

in the second problem are given. The third section is devoted to the formulation of the Cauchy problems as energy error minimization problems, the unknowns being the surface displacement and traction fields on the part of the boundary of the solid where no information is available. A simple example illustrating the method is given in Section 4. The derivation of a closed-form expression for the gradient of the function is given in Section 5, and a link of the present method with the largely used algorithm of Koslov *et al*. (1991), is established in the next section. Finally, Sections 6 and 7 discuss the discretization of the two Cauchy problems with the proposed algorithm and extended 3D numerical examples.

2 Cauchy problems for the Lamé operator

An elastic three-dimensional solid $(\Omega,)$ is considered, the boundary of which is separated into three non-overlapping parts.

- On the first part, denoted by Γ_m, the surface tractions $\boldsymbol{T}^m$ and the displacement field $\boldsymbol{U}^m$ are known (measured),
- On the second part, Γ_b, usual boundary conditions are known (combination of surface tractions and displacement field components); these boundary conditions will be denoted generally by:

$$B\boldsymbol{u} = \boldsymbol{b} \tag{1}$$

- On the third part, Γ_u, the external forces $\boldsymbol{T}^u$ or the displacement $\boldsymbol{U}^u$ are prescribed; **both** of these are unknown.

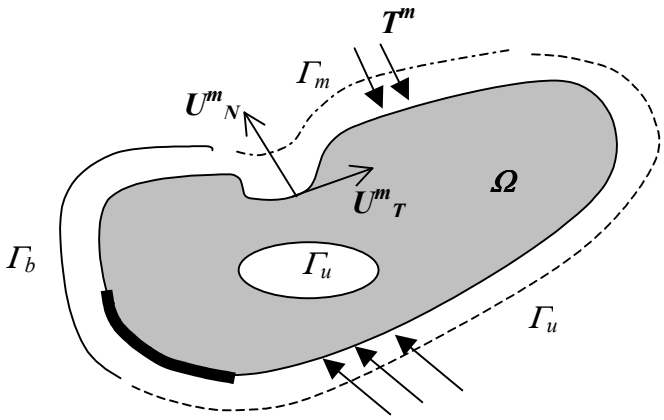

Fig. 1: Definition of the three parts of the boundary

Provided the Hooke's tensor **A** of the elastic material that forms the solid is known, even if possibly dependent on space, with the usual properties ensuring existence and uniqueness of a classical linear elasticity problem, the Cauchy problem and what will be called the incomplete Cauchy problem for the Lamé operator are the following.

Cauchy problem for the Lamé operator:

Given:

The surface traction field $\boldsymbol{T^m}$ and displacement field $\boldsymbol{U^m}$ on Γ_m,

The vector $\boldsymbol{b}$ of usual boundary conditions on Γ_b,

Find the surface tractions $\boldsymbol{T^u}$ and displacement $\boldsymbol{U^u}$ such that an elastic displacement field $\boldsymbol{u}$ exists and satisfies the following equilibrium:

$$\begin{cases} div(\mathbf{A}:\varepsilon(\boldsymbol{u}))=0 & in\ \Omega \\ \mathbf{A}:\varepsilon(\boldsymbol{u}).\boldsymbol{n}=\boldsymbol{T}^m,\ \boldsymbol{u}=\boldsymbol{U}^m & on\ \Gamma_m \\ B\boldsymbol{u}=\boldsymbol{b} & on\ \Gamma_b \\ \mathbf{A}:\varepsilon(\boldsymbol{u}).\boldsymbol{n}=\boldsymbol{T}^u,\ \boldsymbol{u}=\boldsymbol{U}^u & on\ \Gamma_u \end{cases} \tag{2}$$

Incomplete Cauchy problem for the Lamé operator:

Given:

The surface traction field $\boldsymbol{T^m}$ and <u>tangential</u> displacement field $\boldsymbol{U_t^m}$ on Γ_m,

The vector $\boldsymbol{b}$ of usual boundary conditions on Γ_b,

Find the surface tractions $\boldsymbol{T^u}$ and displacement fields $\boldsymbol{U^u}$ such that an elastic equilibrium displacement field $\boldsymbol{u}$ exists and satisfies

$$\begin{cases} div(\mathbf{A}:\varepsilon(\boldsymbol{u}))=0 & in\ \Omega \\ \mathbf{A}:\varepsilon(\boldsymbol{u}).\boldsymbol{n}=\boldsymbol{T}^m,\ \boldsymbol{u}_t=\boldsymbol{U}_t{}^m & on\ \Gamma_m \\ B\boldsymbol{u}=\boldsymbol{b} & on\ \Gamma_b \\ \mathbf{A}:\varepsilon(\boldsymbol{u}).\boldsymbol{n}=\boldsymbol{T}^u,\ \boldsymbol{u}=\boldsymbol{U}^u & on\ \Gamma_u \end{cases} \tag{3}$$

The so-called Incomplete Cauchy Problem defined here is also considered because of the development of image correlation techniques that enable the determination only of tangential displacement fields on stress-free surfaces, which correspond to the conditions on Γ_m considered in (3).

The boundary conditions on parts Γ_m and Γ_u of the solid boundary can be non-linear, as when they involve contact and friction. The only requirements for the application of the Cauchy approach for the Lamé operator is that the linear elasticity assumption is satisfied throughout the solid and that linear boundary conditions appear on the boundary Γ_b.

Existence and uniqueness for the Cauchy problem have been studied extensively for the Laplace operator and more recently for the Lamé operator. The existence is conditioned by a compatibility condition involving the data ($\boldsymbol{U^m}$, $\boldsymbol{T^m}$). This condition is an implicit one but it has been shown that the pairs of compatible data are dense in the space $\left(H^{1/2}(\Gamma_m)\right)^3 \mathrm{x} \left(H^{-1/2}(\Gamma_m)\right)^3$ of all possible data pairs (Fursikov, 2000). This is the reason in most applications that the data are assumed to be

compatible, especially when originating from possibly noisy measurements: each arbitrarily small vicinity of the data pair contains a compatible data pair. A notable exception is the work of Cimetière *et al.* (2001), where the compatibility condition is explicitly tackled in the discrete problem. If compatibly of data is assumed, the Cauchy problem has a unique solution for the Lamé operator with homogeneous and isotropic coefficients (Denman *et al*, 1993, Ang *et al*, 1998).

For the Incomplete Cauchy Problem on an isotropic half-space (or a half-plane in two dimensions), some insights into the question of uniqueness can be gained by using the integral representation of relationships established by Bui (1991), and relating the traction field to the displacement field on the plane x_3=0 delimiting the solid (x_3<0). These relationships read, with the notation y=(x_1, x_2):

$$\sigma_{33}(y,0) = -\frac{2\mu^2}{\lambda+3\mu}\left[u_{1,1}(y,0)+u_{2,2}(y,0)\right] - \frac{\mu(\lambda+2\mu)}{\pi(\lambda+3\mu)}\int_P \frac{u_3(t,0)-u_3(y,0)}{\rho^5(t,y)}dS_t$$

$$\begin{aligned}\sigma_{13}(y,0) = &-\frac{\mu^2}{\pi(\lambda+3\mu)}\int_P \frac{u_1(t,0)-u_1(y,0)}{\rho^3(t,y)}dS_t - \frac{3\mu(\lambda+2\mu)}{2\pi(\lambda+3\mu)}\int_P \frac{u_1(t,0)-u_1(y,0)}{\rho^5(t,y)}(t_1-y_1)^2\,dS_t \\ &+\frac{2\mu^2}{(\lambda+3\mu)}u_{3,1}(y) - \frac{3\mu(\lambda+\mu)}{2\pi(\lambda+3\mu)}\int_P \frac{u_2(t,0)-u_2(y,0)}{\rho^5(t,y)}(t_1-y_1)(t_2-y_2)\,dS_t\end{aligned} \tag{4}$$

$$\begin{aligned}\sigma_{23}(y,0) = &-\frac{\mu^2}{\pi(\lambda+3\mu)}\int_P \frac{u_2(t,0)-u_2(y,0)}{\rho^3(t,y)}dS_t - \frac{3\mu(\lambda+2\mu)}{2\pi(\lambda+3\mu)}\int_P \frac{u_2(t,0)-u_2(y,0)}{\rho^5(t,y)}(t_2-y_2)^2\,dS_t \\ &+\frac{2\mu^2}{(\lambda+3\mu)}u_{3,2}(y) - \frac{3\mu(\lambda+\mu)}{2\pi(\lambda+3\mu)}\int_P \frac{u_1(t,0)-u_1(y,0)}{\rho^5(t,y)}(t_1-y_1)(t_2-y_2)\,dS_t\end{aligned}$$

The integrals appearing in these relations are principal value integrals and $\rho(y,t)=\|y-t\|$. Then, uniqueness for the Incomplete Cauchy Problem is obtained simply by looking at the solution of the elastic problem with vanishing conditions on the plane Γ_m (x_3=0), namely:

$$\begin{cases} div(\mathbf{A}:\varepsilon(\boldsymbol{u}))=0 & in\ \Omega \\ \mathbf{A}:\varepsilon(\boldsymbol{u}).\boldsymbol{n}=0,\ \boldsymbol{u}_T=0 & on\ \Gamma_m \end{cases} \tag{5}$$

Equation (5) leads to the following set of equalities:

$$\begin{aligned}&\sigma_{3i}(y,0)=0 \quad i\in\{1,2,3\} \\ &u_{\alpha,\beta}(y,0)=u_\alpha(y,0)=0 \quad \alpha,\beta\in\{1,2\}^2\end{aligned} \tag{6}$$

and then :

$$u_{3,1}(y,0)=u_{3,2}(y,0) \ \Rightarrow\ u_3(y,0)=Cste$$

The Incomplete Cauchy Problem (up to a translation field parallel to the x_3 axis) reduces to the Cauchy problem for which the uniqueness condition, that is, the unique (null) solution of the homogeneous Cauchy problem, is ensured.

3 Formulation of the Cauchy problems as energy error minimization problems

The general method proposed here to solve the Cauchy problems (2) and (3) is to derive a functional of the unknown fields on Γ_u, say, ($\boldsymbol{\tau}$, $\boldsymbol{v}$), where (possibly local) minima deliver the desired pair of fields ($\boldsymbol{T}^m$, $\boldsymbol{U}^m$). Building this functional follows the two steps below.

First, the two following elastic displacement fields $\boldsymbol{u}_1$ and $\boldsymbol{u}_2$ are defined, as functions respectively of ($\boldsymbol{b}$, $\boldsymbol{U}^m$, $\boldsymbol{\tau}$) and ($\boldsymbol{b}$, $\boldsymbol{T}^m$, $\boldsymbol{v}$). They correspond to the solutions of two well-posed classical mixed elasticity problems.

$$\begin{cases} div(\mathbf{A}:\varepsilon(\boldsymbol{u}_1))=0 & in\ \Omega \\ \boldsymbol{u}_1=\boldsymbol{U}^m & on\ \Gamma_m \\ B\boldsymbol{u}_1=\boldsymbol{b} & on\ \Gamma_b \\ \mathbf{A}:\varepsilon(\boldsymbol{u}_1).\boldsymbol{n}=\boldsymbol{\tau} & on\ \Gamma_u \end{cases} \qquad \begin{cases} div(\mathbf{A}:\varepsilon(\boldsymbol{u}_2))=0 & in\ \Omega \\ \mathbf{A}:\varepsilon(\boldsymbol{u}_2).\boldsymbol{n}=\boldsymbol{T}^m & on\ \Gamma_m \\ B\boldsymbol{u}_2=\boldsymbol{b} & on\ \Gamma_b \\ \boldsymbol{u}_2=\boldsymbol{v} & on\ \Gamma_u \end{cases} \tag{7}$$

For the Incomplete Cauchy Problem there is a slight variation in the definition of the $\boldsymbol{u}_1$ field:

$$\begin{cases} div(\mathbf{A}:\varepsilon(\boldsymbol{u}_1))=0 & in\ \Omega \\ \boldsymbol{u}_1-\boldsymbol{u}_1.\boldsymbol{n}\,\boldsymbol{n}=\boldsymbol{U}_t^m,\ \mathbf{A}:\varepsilon(\boldsymbol{u}_1).\boldsymbol{n}.\boldsymbol{n}=\boldsymbol{T}^m.\boldsymbol{n} & on\ \Gamma_m \\ B\boldsymbol{u}_1=\boldsymbol{b} & on\ \Gamma_b \\ \mathbf{A}:\varepsilon(\boldsymbol{u}_1).\boldsymbol{n}=\boldsymbol{\tau} & on\ \Gamma_u \end{cases} \tag{8}$$

If the boundary condition $B\boldsymbol{u}$ on $\boldsymbol{\Gamma_b}$ contains only prescribed surface tractions, a supplementary condition must be added in the case of plane (or straight) boundary $\boldsymbol{\Gamma_m}$, in order to ensure uniqueness in the elasticity problem (8) :

$$\int_{\Gamma_m} \boldsymbol{u}_1.\boldsymbol{n}\,d\Gamma=0,\ \int_{\Gamma_m} \boldsymbol{u}_1.\boldsymbol{n}\boldsymbol{x}_\alpha\,d\Gamma=0\ \ \alpha=t,v \tag{9}$$

where ($\boldsymbol{t}$, $\boldsymbol{v}$) are two orthogonal vectors in the plane normal to $\boldsymbol{n}$. This condition is unnecessary as soon as the boundary part $\boldsymbol{\Gamma_m}$ contains four non-coplanar points, because it is only added to ensure that the difference $\Delta\boldsymbol{u}_1$of two solutions of (8) vanishes, or (8) from this difference only enjoys :

$$\varepsilon(\Delta\boldsymbol{u}_1)=0,\quad \Delta\boldsymbol{u}_{1T}\big|_{\Gamma_m}=0 \tag{10}$$

It should be noted that the conditions (9) specify a particular choice for the part of the rigid body motion that is kept undetermined in the incomplete Cauchy problem when only surface tractions are prescribed on $\boldsymbol{\Gamma_b}$. Nevertheless, whereas the displacement field $\boldsymbol{u}$ is only determined up to this rigid body motion, the stress field is unique throughout the solid.

Since whenever the two fields $\boldsymbol{u}_1$ and $\boldsymbol{u}_2$ coincide ($\boldsymbol{\tau}$,$\boldsymbol{v}$) is a solution ($\boldsymbol{T}^u$, $\boldsymbol{U}^u$) of the Cauchy problem (2) or (3), the second step consists of the introduction of a functional measuring the gap between the two fields. The choice of this functional here is the error in the semi-norm of elastic energy:

$$\boldsymbol{J}(\boldsymbol{u}_1,\boldsymbol{u}_2)=\frac{1}{2}\int_\Omega \boldsymbol{A}:\varepsilon(\boldsymbol{u}_1-\boldsymbol{u}_2):\varepsilon(\boldsymbol{u}_1-\boldsymbol{u}_2)\,d\Omega \tag{11}$$

The inverse problem is then formulated via the minimization of the energy error functional:

Find ($\boldsymbol{\tau}$, $\boldsymbol{v}$) *that minimize* $E(\boldsymbol{\tau},\boldsymbol{v})$

$$E(\boldsymbol{\tau},\boldsymbol{v}) \equiv \boldsymbol{J}(\boldsymbol{u}_1,\boldsymbol{u}_2) = \frac{1}{2}\int_\Omega \boldsymbol{A} : \varepsilon(\boldsymbol{u}_1 - \boldsymbol{u}_2) : \varepsilon(\boldsymbol{u}_1 - \boldsymbol{u}_2) \tag{12}$$

$$\text{with} \quad \begin{cases} \boldsymbol{u}_1 = \boldsymbol{u}_1(\boldsymbol{b}, \boldsymbol{U}^m, \boldsymbol{\tau}) \ \textit{solution of } (7) \textit{ or } (8) \\ \boldsymbol{u}_2 = \boldsymbol{u}_2(\boldsymbol{b}, \boldsymbol{T}^m, \boldsymbol{v}) \ \textit{solution of } (7) \end{cases}$$

The justification of the formulation lies in the following properties.

Proposition 1:

a) *E* is a positive convex quadratic function,

b) If a pair of fields ($\boldsymbol{\tau}$, $\boldsymbol{v}$) satisfies *E=0* then

i) $\boldsymbol{u}_2 = \boldsymbol{u}_1 + \boldsymbol{R}$, where $\boldsymbol{R}$ is a solid body displacement field
ii) $\boldsymbol{u}_1$ solves the Cauchy problem (2) or (3).

Proof:

The first part of the proposition is obvious because of the affine dependence of the displacement fields $\boldsymbol{u}_1$ and $\boldsymbol{u}_2$ on the data ($\boldsymbol{\tau},\boldsymbol{v}$) , and of the positive nature and convexity of the elastic energy. For the second part, the condition on the field of elastic moduli **A** results in the nullity of the strain associated with $\boldsymbol{u}_2$ - $\boldsymbol{u}_1$ when $\boldsymbol{J}$ vanishes so that the *i)* part follows. The surface tractions on $\boldsymbol{\Gamma_m}$ associated with the displacement field $\boldsymbol{u}_2$ - $\boldsymbol{u}_1$ then also vanish, but owing to equation (7) and to the linearity of the stress-strain elastic relationship, the successive result is:

$$\boldsymbol{0} = \boldsymbol{A} : \varepsilon(\boldsymbol{u}_1 - \boldsymbol{u}_2).\boldsymbol{n} = \boldsymbol{A} : \varepsilon(\boldsymbol{u}_1).\boldsymbol{n} - \boldsymbol{n} : \varepsilon(\boldsymbol{u}_2).\boldsymbol{n} = \boldsymbol{a} : \varepsilon(\boldsymbol{u}_1).\boldsymbol{n} - \boldsymbol{T}^m \quad \textit{on } \Gamma_m$$

This last equality shows that the $\boldsymbol{u}_1$ field satisfies all the desired equations (2) of or (3).

If the data are compatible, the unique minimum of the energy error function is then zero and is reached for the solution of the Cauchy problem. *E* has then a unique minimum. Note also that the above formulation leads to a linear problem (because the function *E* is quadratic); the ill-posedness of the Cauchy problem lies then in the behaviour of the spectrum of the linear operator associated with the (constant) Hessian of the functional: one must expect that the spectrum has zero as an adherence point. Once discretized, this feature will turn out to appear in the bad conditioning of the Hessian matrix, and the condition number is furthermore expected to decrease when the number of unknowns increases. Nevertheless, because of the very high dimension of the unknowns' vector, a direct resolution of the first order optimality condition of the function cannot usually be envisaged, the building of the Hessian matrix being too computationally expensive. A minimization algorithm will be preferred, and the quadratic nature of the function will be exploited when choosing the minimization algorithm to be used.

For computational purpose, an alternative form of the functional can be derived involving only surface integrals, by exploiting the equilibrium properties of the $\boldsymbol{u}$ fields.

Proposition 2:

The functional E is also given by:

$$E(\boldsymbol{\tau},\boldsymbol{v}) = \frac{1}{2}\int_{\Gamma_m} (\boldsymbol{A}:\varepsilon(\boldsymbol{u}_1(\boldsymbol{\tau})).\boldsymbol{n} - \boldsymbol{T}^m).(\boldsymbol{U}^m - \boldsymbol{u}_2(\boldsymbol{v}))d\Gamma + \frac{1}{2}\int_{\Gamma_u} (\boldsymbol{\tau} - \boldsymbol{A}:\varepsilon(\boldsymbol{u}_2(\boldsymbol{v})).\boldsymbol{n}).(\boldsymbol{u}_1(\tau) - \boldsymbol{v})d\Gamma \qquad (13)$$

This last expression is used in the computations and avoids any domain integration. It involves both surfaces Γ_m and Γ_u.

The energy error is very similar to the error in constitutive equation, a concept developed by Ladeveze and co-workers (Ladevèze et al., 1983, 1994 and 1999), see also (Kohn and Mc Kenney, 1990, and Bonnet and Constantinescu, 2005) and used in identification problems (Allix *et al*., 2003, Hadj-Sassi *et al*, 2006), for mesh refinement criteria and *a posteriori* error estimation (Ladeveze *et al*, 1994). Here nevertheless the error involves to displacement fields and not a kinematically admissible displacement field and a statically stress field as in the approaches cited, it can be seen as a dualised version of the error in constitutive equation. It is then possible to derive the boundary expression (13). Furthermore, the error is constructed on the *energy* of the difference field u_1–u_2, this is a consequence of the quadratic character of the elastic energy. For such quadratic potentials it is straightforward to derive the equivalence of this form with the Fenchel residual form, which is the genuine form of the error in constitutive equation for convex potentials:

$$e(\varepsilon_1,\sigma_2) = \varphi(\varepsilon_1) + \varphi^*(\sigma_2) - \sigma_2 : \varepsilon_1$$

Indeed, replacing the stress tensor σ_2 by the associated strain tensor ε_2:

$$\sigma_2 = \boldsymbol{A}:\varepsilon_2$$

One gets:

$$\begin{aligned} e(\varepsilon_1,\varepsilon_2) &= \varphi(\varepsilon_1) + \varphi^*(\mathbf{A}:\varepsilon_2) - \mathbf{A}:\varepsilon_2:\varepsilon_1 \\ &= \frac{1}{2}\mathbf{A}:\varepsilon_1:\varepsilon_1 + \frac{1}{2}\mathbf{A}:\varepsilon_2:\varepsilon_2 - \mathbf{A}:\varepsilon_2:\varepsilon_1 \\ &= \varphi(\varepsilon_1 - \varepsilon_2) \end{aligned}$$

The proposed approach, using the minimization formulation (12), does not incorporate explicitly any kind regularization although the Cauchy problem is very ill posed. Nevertheless the use of conjugate gradient algorithm brings a form of regularization in the numerical applications: the value of the stopping criterion plays the role of regularization parameter. (Bakushinsky *et al.* 2004 and Kokurin 2006). For moderate noise on the data this regularization appears as sufficient as shown for the thermal conductivity equation (Andrieux *et al.* 2006).

4 Analysis of a one-dimensional simple model

To illustrate the flexibility of the proposed approach and to make some comparison with alternative error norms, the following problem is studied. The Cauchy problem is to recover end conditions (u, f) of a pre-tensioned string lying on a Winkler-type foundation, the end conditions at one extremity (T, U) being given.

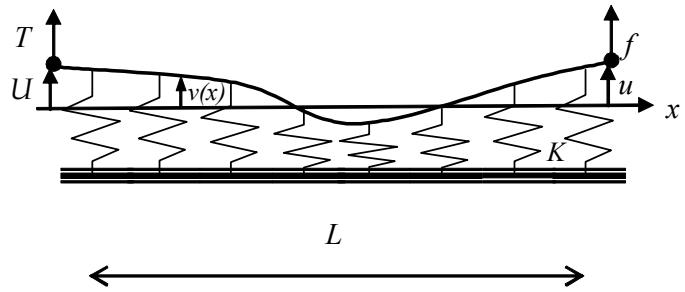

Fig. 2: The Cauchy problem for an elastically supported pre-tensioned string

Denoting by F the tension of the string and by K the spring stiffness density of the foundation, the equilibrium equation involving the vertical displacement v is:

$$\begin{cases} \dfrac{\partial^2 v}{\partial x^2} = k^2 v \quad , \quad 1 < x < L \\ \dfrac{\partial v}{\partial x} = -\dfrac{T}{F}, v = U \quad x = 0 \\ \dfrac{\partial v}{\partial x} = \dfrac{f}{F}, v = u \quad x = L \end{cases} \tag{14}$$

where $k^2 = \dfrac{K}{F}$.

The energy error associated to this problem is:

$$J(v_1, v_2) = \frac{1}{2}\int_0^L \left[\left(v_{1,x} - v_{2,x} \right)^2 + k^2 \left(v_1 - v_2 \right)^2 \right] dx \tag{15}$$

The cost function for the variational approach proposed here for the Cauchy problem is then :

$$2E(\varphi, \upsilon) = -\left[v_{1,x}(0) - v_{2,x}(0) \right].\left[v_1(0) - v_2(0) \right] + \left[v_{1,x}(L) - v_{2,x}(L) \right].\left[v_1(L) - v_2(L) \right] \tag{16}$$

with $$\begin{cases} v_{1,xx} = k^2 v_1 \\ v_1(0) = U \\ v_1, x(L) = \dfrac{\varphi}{F} \end{cases} \quad and \quad \begin{cases} v_{2,xx} = k^2 v_2 \\ v_{2,x}(0) = -\dfrac{T}{F} \\ v_2(L) = \upsilon \end{cases} \tag{17}$$

A closed-form solution for v_1 and v_2 problems leads to the following expression for the function E:

$$\begin{aligned} 2E(\varphi, \upsilon) = &-\left[\frac{\varphi}{F\, th\, kL} - kU\, th\, kL + \frac{T}{F} \right] \left[U - \frac{\upsilon}{ch\, kL} - \frac{T}{kF} th\, kL \right] \\ &+ \left[\frac{\varphi}{F} - k\upsilon\, th\, kL + \frac{T}{F\, ch\, kL} \right] \left[\frac{\varphi}{kF} th\, kL + \frac{U}{ch\, kL} - \upsilon \right] \end{aligned} \tag{18}$$

The Hessian of this quadratic function can be calculated by identifying the quadratic terms of the above expression:

$$HE = th\,kL \begin{bmatrix} \dfrac{1}{kF^2} & \dfrac{-th\,kL}{F} \\ \dfrac{-th\,kL}{F} & k \end{bmatrix}_{(\varphi,\upsilon)} \tag{19}$$

The minimization of the function E is equivalent to the resolution of the linear problem:

$$HE \begin{bmatrix} \varphi \\ v \end{bmatrix} = \begin{bmatrix} f(U,T) \\ g(U,T) \end{bmatrix}$$

so that, although the one-dimensional Cauchy problem is well-posed for $K>0$ and a finite string length, the general ill-posed character of Cauchy problems is revealed in the condition number of the Hessian of the quadratic E function, in the non-dimensional variables $(\tilde{\varphi},\tilde{\upsilon}) = (\dfrac{\varphi}{F}, k\upsilon)$:

$$cond(\tilde{H}E) = cond\left(\frac{th\,kL}{k} \begin{bmatrix} 1 & -th\,kL \\ -th\,kL & 1 \end{bmatrix}_{(\tilde{\varphi},\tilde{\upsilon})}\right) = \frac{1-th\,kL}{1+th\,kL} \tag{20}$$

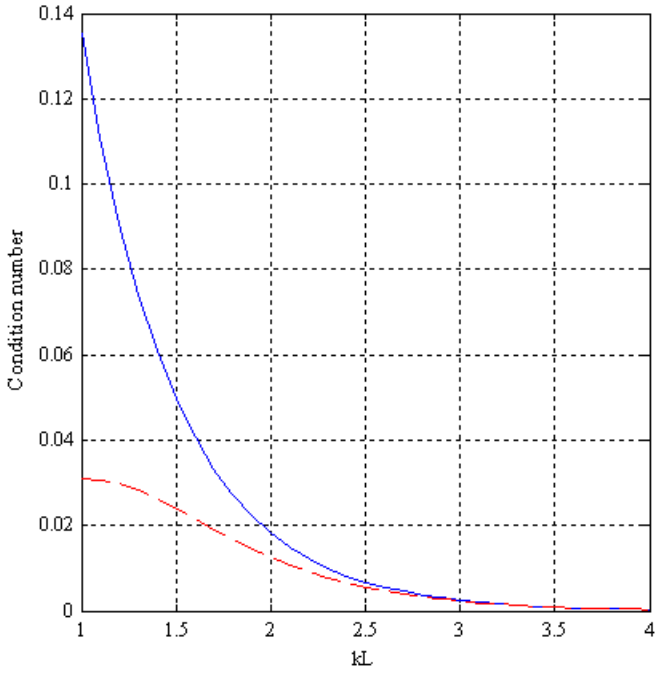

Fig. 3: Condition number of the Hessian of the E (heavy line) and the LS (dotted line) function as a function of the kL parameter of the elastically supported string.

As physically expected and illustrated on figure 3, the problem becomes ill-posed when the length of the string or the stiffness of the foundation increases and when the pretension of the string decreases.

This simple example enables us also to compare the merits of the energy function E based on the J norm (15), which is the energy norm of the problem under consideration, and of a functional based on a simple L^2 -norm on the displacement, in this case the least-square error:

$$LS(\varphi,\upsilon)=\frac{1}{2}\int_0^L\left[\left(v_1(\varphi)-v_2(\upsilon)\right)^2\right]dx \tag{21}$$

Figure 4 clearly shows that the energy-based error norm exhibits better behaviour with respect to convexity and conditioning than the least-square-based function.

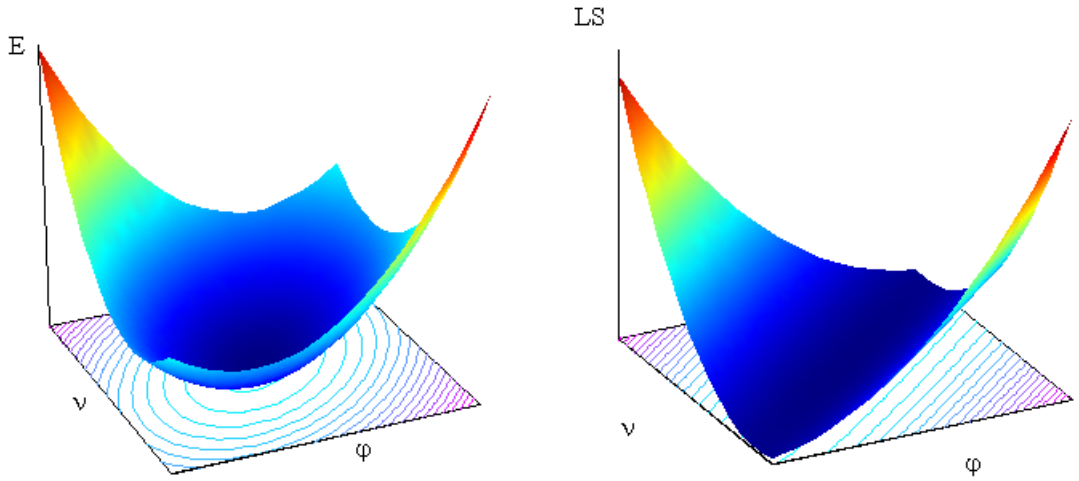

Fig. 4. Levels of the E function (left) and the LS function (right) in the (υ,φ) plane (kL=2)

This observation can be confirmed by figure 3, which compares the condition numbers of the Hessian of the two functions.

5 Computing the gradient of the energy error function by the adjoint fields method

The minimization problem (12) can be reduced to a linear equation solution because the E functional is quadratic. Once the unknown fields are discretized, under the following form

$$\boldsymbol{\tau}(x)=\sum_{i=1}^{m}\tau_i\Phi^i(x),\ \boldsymbol{\upsilon}(x)=\sum_{\alpha=1}^{n}\upsilon_\alpha\Psi^\alpha(x) \tag{22}$$

the unknowns or design variables of the Cauchy problem will be gathered into a vector X= (τ_i,υ_α) of IR^N, $i=1,..m$, $a=1,..,n$, $N=m+n$. For a small dimension N of the unknown vector, a direct approach may be preferable to the optimization approach. The first step is the building of the Hessian (constant) matrix associated with the E function, and the left-hand side of the first order optimization condition for E :

$$H.X=F \tag{23}$$

For that purpose, the following elementary field $\boldsymbol{u}^*$ must be computed:

$$\begin{cases} div(\mathbf{A}:\varepsilon(\boldsymbol{u}^*_{1i}))=0 & in\ \Omega \\ \boldsymbol{u}^*_{1i}= & on\ \Gamma_m \\ B\boldsymbol{u}^*_{1i}=\boldsymbol{0} & on\ \Gamma_b \\ \mathbf{A}:\varepsilon(\boldsymbol{u}^*_{1i}).\boldsymbol{n}=\Phi' & on\ \Gamma_u \end{cases} \qquad \begin{cases} div(\mathbf{A}:\varepsilon(\boldsymbol{u}^*_{2\alpha}))=0 & in\ \Omega \\ \mathbf{A}:\varepsilon(\boldsymbol{u}^*_{2\alpha}).\boldsymbol{n}=0 & on\ \Gamma_m \\ B\boldsymbol{u}^*_{2\alpha}=\boldsymbol{0} & on\ \Gamma_b \\ \boldsymbol{u}_{2\alpha}=\Psi^{\alpha} & on\ \Gamma_u \end{cases} \tag{24}$$

Then, using the two supplementary fields $\boldsymbol{u}^0_1$ and $\boldsymbol{u}^0_2$:

$$\begin{cases} div(\mathbf{A}:\varepsilon(\boldsymbol{u}^0_1))=0 & in\ \Omega \\ \boldsymbol{u}^0_1=\boldsymbol{U}^m & on\ \Gamma_m \\ B\boldsymbol{u}^0_1=\boldsymbol{b} & on\ \Gamma_b \\ \mathbf{A}:\varepsilon(\boldsymbol{u}^0_1).\boldsymbol{n}=\boldsymbol{0} & on\ \Gamma_u \end{cases} \qquad \begin{cases} div(\mathbf{A}:\varepsilon(\boldsymbol{u}^0_2))=0 & in\ \Omega \\ \mathbf{A}:\varepsilon(\boldsymbol{u}^0_2).\boldsymbol{n}=\boldsymbol{T}^m & on\ \Gamma_m \\ B\boldsymbol{u}^0_2=\boldsymbol{b} & on\ \Gamma_b \\ \boldsymbol{u}^0_2=\boldsymbol{0} & on\ \Gamma_u \end{cases} \tag{25}$$

the Hessian and the left-hand side of (23) are :

$$H_{ij}=J(\boldsymbol{u}^*_{1i},\boldsymbol{u}^*_{1j})\ ,\ H_{i\alpha}=J(\boldsymbol{u}^*_{1i},\boldsymbol{u}^*_{2\alpha})\ ,\ H_{\alpha\beta}=-J(\boldsymbol{u}^*_{2\alpha},\boldsymbol{u}^*_{2\beta}) \tag{26}$$

$$F_i=J(\boldsymbol{u}^*_{1i},\boldsymbol{u}^0_1-\boldsymbol{u}^0_2)\ ,\ F_{\alpha}=J(\boldsymbol{u}^*_{2\alpha},\boldsymbol{u}^0_2-\boldsymbol{u}^0_1) \tag{27}$$

The direct resolution method (23) is different from the direct approach of Brian *et al.* (2004), which uses permutations, rearrangements and partial inversions of the discretized system of equations associated with the Cauchy problem (2).

Nevertheless, the building of the Hessian matrix *H* associated with the function must be avoided for large-scale problems (*N* large) because of prohibitive computational costs (*N*+2 resolution of the direct problem, even if advantage can be taken of there being only two distinct stiffness matrices to deal with). Furthermore, the *H* matrix being full, the costs of direct resolution of (23) increase rapidly. (Note also that the ill-conditioning of it precludes any iterative method for the linear system). A direct optimization method should be preferred, using only the gradients of the function. The gradient has to be computed by an adjoint method because of the implicit dependence of the $\boldsymbol{u}_1$ and $\boldsymbol{u}_2$ fields with respect to the variables, and the relatively high cost of evaluation of the function itself (Chavent, 1991, Griewank, 1993).

Recall the form of the *E* function and the so-called state equation associated with fields $\boldsymbol{u}_1$ and $\boldsymbol{u}_2$ for the Cauchy Problem:

$$E(\boldsymbol{\tau},\boldsymbol{v})\equiv J(\boldsymbol{u}_1,\boldsymbol{u}_2)=\frac{1}{2}\int_{\Omega}\boldsymbol{A}:\varepsilon(\boldsymbol{u}_1-\boldsymbol{u}_2):\varepsilon(\boldsymbol{u}_1-\boldsymbol{u}_2) \tag{28}$$

with

$$\begin{cases} div(\mathbf{A}:\varepsilon(\boldsymbol{u}_1))=0 & in\ \Omega \\ \boldsymbol{u}_1=\boldsymbol{U}^m & on\ \Gamma_m \\ B\boldsymbol{u}_1=\boldsymbol{b} & on\ \Gamma_b \\ \mathbf{A}:\varepsilon(\boldsymbol{u}_1).\boldsymbol{n}=\boldsymbol{\tau} & on\ \Gamma_u \end{cases} \qquad \begin{cases} div(\mathbf{A}:\varepsilon(\boldsymbol{u}_2))=0 & in\ \Omega \\ \mathbf{A}:\varepsilon(\boldsymbol{u}_2).\boldsymbol{n}=\boldsymbol{T}^m & on\ \Gamma_m \\ B\boldsymbol{u}_2=\boldsymbol{b} & on\ \Gamma_b \\ \boldsymbol{u}_2=\boldsymbol{v} & on\ \Gamma_u \end{cases} \tag{29}$$

The Lagrangian associated with the energy error function and with the state equations is :

$$L(\boldsymbol{u}_1,\boldsymbol{u}_2,\boldsymbol{\mu},\boldsymbol{\lambda},\boldsymbol{v}_1,\boldsymbol{v}_2;\boldsymbol{\tau},\upsilon) = J(\boldsymbol{u}_1,\boldsymbol{u}_2) + \int_\Omega \left[\boldsymbol{A}:\varepsilon(\boldsymbol{u}_1):\varepsilon(\boldsymbol{v}_1) + \boldsymbol{A}:\varepsilon(\boldsymbol{u}_2):\varepsilon(\boldsymbol{v}_2)\right] d\Omega$$
$$-\int_{\Gamma_m} \boldsymbol{T}^m.\boldsymbol{v}_2 d\Gamma_m - \int_{\Gamma_u} \left[\boldsymbol{\lambda}.(\boldsymbol{u}_2-\upsilon) + \boldsymbol{\mu}.\boldsymbol{v}_2 + \boldsymbol{\tau}.\boldsymbol{v}_1\right] d\Gamma_i \qquad (30)$$
$$-\int_{\Gamma_b} \boldsymbol{b}.(\boldsymbol{v}_1+\boldsymbol{v}_2) d\Gamma_b$$

which is defined on the following product space :

$$(\boldsymbol{u}_1,\boldsymbol{u}_2,\boldsymbol{v}_1,\boldsymbol{v}_2,\boldsymbol{\lambda},\boldsymbol{\mu}) \in U_1 \mathrm{x}\, H^1(\Omega)^3 \,\mathrm{x}\, U_1^0 \,\mathrm{x}\, H^1(\Omega)^3 \,\mathrm{x}\, H^{-1/2}(\Gamma_u)^3 \,\mathrm{x}\, H^{-1/2}(\Gamma_u)^3 \qquad (31)$$

with : $U_1 = \left\{\boldsymbol{u} \in H^1(\Omega)^3,\ \boldsymbol{u}\big|_{\Gamma_m} = \boldsymbol{U}^m\right\},\ U_1^0 = \left\{\boldsymbol{v} \in H^1(\Omega)^3,\ \boldsymbol{v}\big|_{\Gamma_m} = 0\right\}$

Following the classical approach, the stationarity of the Lagrangian with respect to primal fields $\boldsymbol{u_1}$ and $\boldsymbol{u_2}$ leads to the definition of the two adjoint problems:

$$\begin{cases} div(\mathbf{A}:\varepsilon(\boldsymbol{v}_1)) = 0 & in\ \Omega \\ \boldsymbol{v}_1 = 0 & on\ \Gamma_m \\ \mathbf{A}:\varepsilon(\boldsymbol{v}_1).\boldsymbol{n} = \boldsymbol{0} & on\ \Gamma_b \\ \mathbf{A}:\varepsilon(\boldsymbol{v}_1).\boldsymbol{n} = \mathbf{A}:\varepsilon(\boldsymbol{u}_2).\boldsymbol{n} - \boldsymbol{\tau} & on\ \Gamma_u \end{cases} \qquad \begin{cases} div(\mathbf{A}:\varepsilon(\boldsymbol{v}_2)) = 0 & in\ \Omega \\ \mathbf{A}:\varepsilon(\boldsymbol{v}_2).\boldsymbol{n} = \mathbf{A}:\varepsilon(\boldsymbol{u}_1).\boldsymbol{n} - \boldsymbol{T}^m & on\ \Gamma_m \\ \mathbf{A}:\varepsilon(\boldsymbol{v}_2).\boldsymbol{n} = \boldsymbol{0} & on\ \Gamma_b \\ \boldsymbol{v}_2 = 0 & on\ \Gamma_u \end{cases} \qquad (32)$$

These adjoint problems are quite simple; because of the self-adjoint character of the Lamé operator, they are also linear elasticity problems, and because of the energy choice for the semi-norm used in the measure of the gap between $\boldsymbol{u_1}$ and $\boldsymbol{u_2}$, only boundary conditions involving the data and the primal fields appear. Equipped with these adjoint fields, the gradients of the error functional are simply:

$$\nabla_{\boldsymbol{\tau}} E(\boldsymbol{\tau},\boldsymbol{\upsilon}) = -\boldsymbol{v}_1\big|_{\Gamma_u} \quad , \quad \nabla_{\boldsymbol{\upsilon}} E(\boldsymbol{\tau},\boldsymbol{\upsilon}) = \left[\boldsymbol{A}:(\boldsymbol{u}_2).n + \boldsymbol{A}:(\boldsymbol{v}_2).n - \boldsymbol{\tau}\right]\big|_{\Gamma_u} \qquad (33)$$

In these equations, the interpretation of the Lagrange multiplier $\boldsymbol{\lambda}$ obtained from the stationary condition of the Lagrangian with respect to primal field $\boldsymbol{u_2}$ has been taken into account in order to derive expressions involving only the $\boldsymbol{v_2}$ and $\boldsymbol{u_2}$ fields.

For the Incomplete Cauchy Problem, similar results hold with only two minor modifications in the vector spaces of the $\boldsymbol{u_1}$ and $\boldsymbol{v_1}$ fields that become:

$$U_1 = \left\{\boldsymbol{u} \in H^1(\Omega)^3,\ \boldsymbol{u} - \boldsymbol{u}.n\,n\big|_{\Gamma_m} = \boldsymbol{U}_t^m\right\},\ U_1^0 = \left\{\boldsymbol{v} \in H^1(\Omega)^3,\ \boldsymbol{v} - \boldsymbol{v}.n\,n\big|_{\Gamma_m} = 0\right\}$$

and in the definition of the adjoint field $\boldsymbol{v_1}$, namely:

$$\begin{cases} div(\mathbf{A}:\varepsilon(\boldsymbol{v}_1)) = 0 & in\ \Omega \\ \boldsymbol{v}_1 - \boldsymbol{v}_1.\boldsymbol{n}\,\boldsymbol{n} = 0, \mathbf{A}:\varepsilon(\boldsymbol{v}_1).\boldsymbol{n}.\boldsymbol{n} = 0 & on\ \Gamma_m \\ \mathbf{A}:\varepsilon(\boldsymbol{v}_1).\boldsymbol{n} = \boldsymbol{0} & on\ \Gamma_b \\ \mathbf{A}:\varepsilon(\boldsymbol{v}_1).\boldsymbol{n} = \mathbf{A}:\varepsilon(\boldsymbol{u}_2).\boldsymbol{n} - \boldsymbol{\tau} & on\ \Gamma_u \end{cases}$$

6 Minimization algorithm and link with the *Kozlov–Maz'ya–Fomin* alternating algorithm

The method proposed in this work can be related to that introduced by Kozlov *et al* (1991) and widely numerically studied by Lesnic *et al* (2004) and references therein. In that approach, the data completion problem is solved on the basis of an alternating iterative procedure, where successive solutions of well-posed mixed boundary value problems for the original equation are computed. The method has been proven to be convergent (Kozlov *et al* (1991), Baumeister *et al* (2001)). Here, the approach generalizes that of Kozlov *et al*. (KMF algorithm) in the following sense as shown below: it is simply an alternating-direction minimization method of the error function E, the successive directions being those of the displacement (Dirichlet) unknown $\boldsymbol{v}$ and the surface traction (Neumann) unknown $\boldsymbol{\tau}$. For compatible data, the strict convexity of the E function then leads to a new proof of the convergence of this algorithm.

Indeed, starting from the equation (2), instead of simultaneously using two solutions of a well-posed problem, the iterative KMF algorithm uses two kinds of well-posed problems, each of them defining a sub-iteration. At iteration $2k+1$, the following problem is solved, provided a field $\boldsymbol{u}^{2k}$ is given:

$$\begin{cases} div(\mathbf{A}:\varepsilon(\boldsymbol{u}^{2k+1}))=0 & in\ \Omega \\ \boldsymbol{u}^{2k+1}=\boldsymbol{U}^{\boldsymbol{m}} & on\ \Gamma_m \\ B\boldsymbol{u}^{2k+1}=\boldsymbol{b} & on\ \Gamma_b \\ \mathbf{A}:\varepsilon(\boldsymbol{u}^{2k+1}).\boldsymbol{n}=\mathbf{A}:\varepsilon(\boldsymbol{u}^{2k}).\boldsymbol{n} & on\ \Gamma_u \end{cases} \tag{34}$$

Then the iteration $2k+2$ is performed by solving:

$$\begin{cases} div(\mathbf{A}:\varepsilon(\boldsymbol{u}^{2k+2}))=0 & in\ \Omega \\ \mathbf{A}:\varepsilon(\boldsymbol{u}^{2k+2}).\boldsymbol{n}=\boldsymbol{T}^{\boldsymbol{m}} & on\ \Gamma_m \\ B\boldsymbol{u}^{2k+2}=\boldsymbol{b} & on\ \Gamma_b \\ \boldsymbol{u}^{2k+2}=\boldsymbol{u}^{2k+1} & on\ \Gamma_u \end{cases} \tag{35}$$

The algorithm is then a fixed-point algorithm: when the difference of two successive solutions $\boldsymbol{u}^{2k}$ and $\boldsymbol{u}^{2k+1}$ vanishes, then the Cauchy problem is solved. The link with the present method can be established through the following properties of the solutions of each sub-iteration.

$$\begin{aligned} &\boldsymbol{u}^{2k+1}=\boldsymbol{u}_1(\overline{\boldsymbol{\tau}}) \Leftrightarrow \overline{\boldsymbol{\tau}}=ArgMin\,E(\boldsymbol{\tau},\boldsymbol{v}^{2k}) \ \ with\ \boldsymbol{v}^{2k}=\boldsymbol{u}^{2k}\,|_{\Gamma_u} \\ &\boldsymbol{u}^{2k+2}=\boldsymbol{u}_2(\overline{\boldsymbol{v}}) \Leftrightarrow \overline{\boldsymbol{v}}=ArgMin\,E(\boldsymbol{\tau}^{2k+1},\boldsymbol{v}) \ \ with\ \boldsymbol{\tau}^{2k+1}=\mathbf{A}:(\varepsilon(\boldsymbol{u}^{2k+1})\cdot\boldsymbol{n}\,|_{\Gamma_u} \end{aligned} \tag{36}$$

The proof of these results follows exactly the same lines as for the Cauchy Problem for the Laplace equation, addressed in Andrieux *et al* (2006), which is not given here. This result clarifies that far better performances are achieved using the present method, as observed in the numerical applications described in the last part of the paper; this improvement is attributable to use of a more efficient optimization algorithm than the alternating direction method.

The minimization of the E function can take advantage of its quadratic feature. Namely, conjugate gradient algorithm will be preferred and naturally designed for such an optimization, without explicitly building the constant Hessian Matrix. However, attention must be paid to the bad conditioning, due to the ill-posedness of the Cauchy Problem itself, even if better conditioning is to

be expected by comparison to other functions as exemplified in part 8 of this paper. To deal with this issue, a more specific algorithm, the Trust Region Method (TRM), is used.

7 Discretization

The implementation of the above method was carried out using the finite element method (FEM). Hence, the derivation of the adjoint state is preferably established on the basis of the FEM-discretized problem. The advantage of this fully discrete approach is that the exact gradient of the discrete objective function is obtained; moreover, it is easily implementable. We describe here only the Cauchy Problem; modifications for the Incomplete Cauchy Problem are straightforward.

We consider a mesh of Ω characterized by n nodes. We denote by p the number of nodes on the boundary Γ_u and by q the number of nodes on the boundary Γ_m. Using Lagrange multipliers to formulate the Dirichlet boundary conditions, the discretized forms of problems (7) are as follows:

$$\begin{bmatrix} K & L_m^T \\ L_m & 0 \end{bmatrix} \begin{Bmatrix} U_1 \\ p_1 \end{Bmatrix} = \begin{Bmatrix} F_1 \\ U^m \end{Bmatrix} \quad and \quad \begin{bmatrix} K & L_u^T \\ L_u & 0 \end{bmatrix} \begin{Bmatrix} U_2 \\ p_2 \end{Bmatrix} = \begin{Bmatrix} F_2 \\ X_{\boldsymbol{\upsilon}} \end{Bmatrix} \tag{37}$$

where K is the overall $n \times n$ stiffness matrix, U_1 and U_2 are the nodal variable vectors and F_1 and F_2 are the load vectors. $\{p_1\}$ and $\{p_2\}$ are the unknown nodal forces related to the degrees of freedom on Γ_m and Γ_u, respectively. The entries of the indicated rectangular $q \times n$ matrix L_m and $p \times n$ matrix L_u are *1* and *0* such that $L_m U_1 = U^m$ and $L_u U_2 = X_{\boldsymbol{\upsilon}}$. U^m denotes the discretized form of $\boldsymbol{U}^{\mathrm{m}}$.

$F_1 = \{X_\tau, 0\}^T$ is the load vector, where X_τ contains the unknown nodal loads on Γ_u and depends explicitly on τ. The components of U_1 defined on Γ_m are fixed and depend on $\boldsymbol{U}^{\mathrm{m}}$, the others depend implicitly on τ and $\boldsymbol{U}^{\mathrm{m}}$. Likewise, $U_2 = \{X_{\boldsymbol{\upsilon}}, \hat{U}_2\}^T$, where $X_{\boldsymbol{\upsilon}}$ gathers the prescribed nodal variables associated with $\boldsymbol{\upsilon}$, while $\hat{U}_2$ collects all nodal variables left unknown by the boundary conditions of the second problem of (7). The components of the load vector F_2 defined on Γ_m are prescribed and depend on T^m; the others are null. The components of the load vector p_1 are unknown and depend on X_τ and $\boldsymbol{U}^{\mathrm{m}}$, although those of p_2 which are unknown depend on $X_{\boldsymbol{\upsilon}}$ and T^m.

However, matrix K is fixed. Then, X_τ and $X_{\boldsymbol{\upsilon}}$ are the discretized design variables of the optimization problem (12) described above. The energy function, in its discretized form, can be written as follows:

$$\begin{aligned} E(X_\eta, X_\tau) &= \frac{1}{2}\left(U_1 - U_2\right)^T \cdot K \left(U_1 - U_2\right) \\ &= \frac{1}{2}\left(U_1 - U_2\right)^T \cdot \left(F_1 - L_m^T p_1 - F_2 + L_u^T p_2\right) \end{aligned} \tag{38}$$

The discrete optimization problem is then stated as follows:

$$\begin{aligned} &\min_{(X_\tau, X_\upsilon)} E\left(X_\tau, X_\upsilon\right) \\ &with: \\ &\begin{bmatrix} K & L_m^T \\ L_m & 0 \end{bmatrix} \begin{Bmatrix} U_1 \\ p_1 \end{Bmatrix} = \begin{Bmatrix} F_1 \\ U^m \end{Bmatrix} \quad and \quad \begin{bmatrix} K & L_u^T \\ L_u & 0 \end{bmatrix} \begin{Bmatrix} U_2 \\ p_2 \end{Bmatrix} = \begin{Bmatrix} F_2 \\ X_\upsilon \end{Bmatrix} \end{aligned} \tag{39}$$

The adjoint method was used to evaluate the derivatives of E. A Lagrangian is defined as follows:

$$L(U_1,U_2,\lambda_1,\lambda_2,q_1,q_2,p_1,p_2,X_\tau,X_\upsilon) = E(U_1(X_\tau),U_2(X_\upsilon))$$
$$-\begin{Bmatrix}\lambda_1\\ q_1\end{Bmatrix}^T\left\{\begin{bmatrix}K & L_m^T\\ L_m & 0\end{bmatrix}\begin{Bmatrix}U_1\\ p_1\end{Bmatrix}-\begin{Bmatrix}F_1\\ U^m\end{Bmatrix}\right\}-\begin{Bmatrix}\lambda_2\\ q_2\end{Bmatrix}^T\left\{\begin{bmatrix}K & L_u^T\\ L_u & 0\end{bmatrix}\begin{Bmatrix}U_2\\ p_2\end{Bmatrix}-\begin{Bmatrix}F_2\\ X_\upsilon\end{Bmatrix}\right\} \tag{40}$$

where the vectors of Lagrange multipliers λ_i and q_i are virtual displacements and nodal forces, respectively. By virtue of (37),

$$\frac{dL}{dX_\tau} = \frac{dE}{dX_\tau} \tag{41}$$

$$\frac{dL}{dX_\upsilon} = \frac{dE}{\partial X_\upsilon} \tag{42}$$

Differentiation of (40) with respect to the design parameters yields:

$$\frac{dL}{dX_\tau} = \frac{\partial E}{\partial U_1}\frac{dU_1}{dX_\tau} - \begin{Bmatrix}\lambda_1\\ q_1\end{Bmatrix}^T\left(\left\{\begin{bmatrix}K & L_m^T\\ L_m & 0\end{bmatrix}\begin{Bmatrix}\frac{dU_1}{dX_\tau}\\ \frac{dp_1}{dX_\tau}\end{Bmatrix}-\begin{Bmatrix}\frac{dF_1}{dX_\tau}\\ 0\end{Bmatrix}\right\}\right) \tag{43}$$

$$\frac{dL}{dX_\upsilon} = \frac{\partial E}{\partial U_2}\frac{dU_2}{dX_\upsilon} - \begin{Bmatrix}\lambda_2\\ q_2\end{Bmatrix}^T\left\{\begin{bmatrix}K & L_u^T\\ L_u & 0\end{bmatrix}\begin{Bmatrix}\frac{dU_2}{dX_\upsilon}\\ \frac{dp_2}{dX_\upsilon}\end{Bmatrix}-\begin{Bmatrix}0\\ I_{p\times p}\end{Bmatrix}\right\} \tag{44}$$

where $I_{p\times p}$ denotes the $p\times p$ square identity matrix. The derivative (41) can be written as follows:

$$\frac{\partial L}{\partial X_\tau} = \left\{\begin{Bmatrix}\frac{\partial E}{\partial X_\tau}\\ 0\end{Bmatrix}-\begin{Bmatrix}\lambda_1\\ q_1\end{Bmatrix}^T\begin{bmatrix}K & L_m^T\\ L_m & 0\end{bmatrix}\right\}\begin{Bmatrix}\frac{dU_1}{dX_\tau}\\ \frac{dp_1}{dX_\tau}\end{Bmatrix}+\begin{Bmatrix}\lambda_1\\ q_1\end{Bmatrix}^T\begin{Bmatrix}\frac{dF_1}{dX_\tau}\\ 0\end{Bmatrix} \tag{45}$$

where the implicit derivatives can be eliminated by selecting λ_1 such that the term in the round bracket is cancelled. This is achieved if λ_1 solves the following system:

$$\begin{bmatrix}K & L_m^T\\ L_m & 0\end{bmatrix}\begin{Bmatrix}\lambda_1\\ q_1\end{Bmatrix}^T = \begin{Bmatrix}\frac{\partial E}{\partial X_\tau}\\ 0\end{Bmatrix} = \begin{Bmatrix}K(U_1-U_2)\\ 0\end{Bmatrix} \tag{46}$$

The system (46) is referred to as the adjoint problem for the adjoint response λ_1 with the adjoint load $\partial E / \partial U_1$ and the adjoint Dirichlet boundary condition $\lambda_1 = 0$ on Γ_m. Once multipliers λ_1 are evaluated, the derivatives of E with respect to the specific parameters X_τ are obtained by:

$$\frac{dE}{dX_\tau} = \begin{Bmatrix} \lambda_1 \\ q_1 \end{Bmatrix}^T \begin{Bmatrix} \frac{dF_1}{dX_\tau} \\ 0 \end{Bmatrix} = \begin{Bmatrix} \lambda_1 \\ q_1 \end{Bmatrix}^T \begin{Bmatrix} I_{p\times p} \\ 0 \end{Bmatrix} = \lambda_1^T |_{\Gamma_u} \tag{47}$$

The derivative (42) can be written as follows:

$$\frac{dL}{dX_\upsilon} = \left\{ \begin{Bmatrix} \frac{\partial E}{\partial U_2} \\ 0 \end{Bmatrix} - \begin{Bmatrix} \lambda_2 \\ q_2 \end{Bmatrix}^T \begin{bmatrix} K & L_u^T \\ L_u & 0 \end{bmatrix} \right\} \begin{Bmatrix} \frac{dU_2}{dX_\upsilon} \\ \frac{dp_2}{dX_\upsilon} \end{Bmatrix} + \begin{Bmatrix} \lambda_2 \\ q_2 \end{Bmatrix}^T \begin{Bmatrix} 0 \\ I_{p\times p} \end{Bmatrix} \tag{48}$$

In this case, λ_2 is defined so that the first term in round brackets in equation (48) is cancelled. This is achieved if λ_2 solves the following system:

$$\begin{bmatrix} K & L_u^T \\ L_u & 0 \end{bmatrix} \begin{Bmatrix} \lambda_2 \\ q_2 \end{Bmatrix} = \begin{Bmatrix} \frac{\partial E}{\partial U_2} \\ 0 \end{Bmatrix} = \begin{Bmatrix} K(U_2 - U_1) \\ 0 \end{Bmatrix} \tag{49}$$

The system (49) is referred to as the adjoint problem for the adjoint response λ_2 with the adjoint load $\partial E / \partial U_2$ and the adjoint Dirichlet boundary condition $\lambda_2 = 0$ on Γ_u. Once multipliers λ_2 are evaluated, q_2 can be expressed as follows:

$$L_u^T q_2 = \frac{\partial E}{\partial X_\upsilon} - K\lambda_2 = K(U_2 - U_1) - K\lambda_2 \tag{50}$$

Then, the derivatives of E with respect to the specific parameters X_τ are obtained by:

$$\frac{dE}{dX_\upsilon} = \begin{Bmatrix} \lambda_2 \\ q_2 \end{Bmatrix}^T \begin{Bmatrix} 0 \\ I_{p\times p} \end{Bmatrix} = L_u^T q_2 |_{\Gamma_u} = K\left(U_2 - U_1 - \lambda_2\right)|_{\Gamma_u} \tag{51}$$

These formulas, (46), (49), (47) and (51), represent the discrete counterpart of the continuum results (32) and (33). The adjoint method requires the solution of two adjoint problems for each response function E; it is efficient when the number of functions and constraints is small compared to the number of design parameters. This clearly the case here, as the design parameters are fields defined on a part of the boundary of the mesh.

Going back to the minimization algorithm for the discretized E function, each iteration of the algorithm involves the solution of four linear systems: two direct problems defined in (37) and two adjoint problems defined by (46) and (49). The energy function can be written formally as follows:

$$E(X)=\frac{1}{2}X^T HX+X^T B+C$$
$$with \quad X^T=\left\{X_\tau^T, X_\upsilon^T\right\} \tag{52}$$

where H is the Hessian which depends only on the geometric and material data, while B and C depend on the geometric and material data and also on the measured boundary data ($\boldsymbol{T}^m$, $\boldsymbol{U}^m$). The Hessian is positive and undefined, and so the convergence of the conjugate gradient algorithm is slow. In order to optimize the computational cost the Trust Region Method (TRM) is adopted. This last method must solve the following subproblem for each iteration k:

$$\min\left\{Q(S_k)=\frac{1}{2}S_k^T HS_k+S_k^T\nabla E_{k-1} \;\; such\ that \left\|S_k^T\right\|\le\delta\right\} \tag{53}$$

where $Q(S_k)$ is the quadratic approximation of $E(X_{k-1}+S_k)$, $\nabla E_{k-1}=HX_{k-1}+B$ is the energy function gradient computed at the preceding iteration $(k-1)$, and δ is a positive scalar the size of the trust region and reflects the confidence in the second-order model. As the energy function E is quadratic, $Q(S_k)$ is an exact approximation of $E(X_{k-1}+S_k)$, and the optimal search direction is the Newton one: $S_k=-H^{-1}\nabla E_{k-1}$. However, when the Hessian is singular and the gradient depends on the overspecified data, then this search direction is not well defined. The search direction is instead defined by solving the Trust Region Subproblem defined by (53), whose associated Lagrangian function is:

$$\mathcal{L}(X,\lambda)=\frac{1}{2}S_k^T HS_k+S_k^T\Delta E_{k-1}+\frac{\lambda}{2}S_k^T S_k \tag{54}$$

This quadratic function can be interpreted as a regularized quadratic model for E around X_{k-1}, and its exact solution is given by:

$$\left(H+\lambda I\right)S_k=-\nabla E_{k-1} \tag{55}$$

The algorithm used in this study is similar to the one implemented in the *optimization toolbox* of Matlab. The approximation approach followed is to restrict the Trust-Region Subproblem to a two-dimensional subspace (Byrd *et al*., 1988, Coleman *et al*., 1996).

8 Numerical applications

The performance and accuracy of the proposed method has been investigated through numerical three-dimensional examples where the measured data are extracted from the results of the direct problems. The first application deals with the identification of the indentation pressure of a heterogeneous solid, and the second one with the identification of contact area between two elastic solids.

8.1 Identification of indentation pressure on a two-layer solid.

The first example addresses the indentation of a solid composed of two layers of different materials (steel and titanium). This solid is shown in figure 1 where, thanks to symmetry, only a quarter of the solid has been modelled. The problem is stated as follows:

- ✓ Overspecified data: displacements and surface traction are known on the rectangular area denoted by Γ_m.
- ✓ Boundary Γ_b gathering the four side faces: two have Dirichlet boundary conditions of symmetry, whereas the other two are free from surface tractions and correspond, then, to null Neumann boundary conditions.
- ✓ Boundary Γ_u where the data are unknown includes the remaining faces (the bottom face and the remaining area of the top face).
- ✓ Elastic parameters: Layer 1 is steel with $E_s=2.1\ 10^{11}\ Pa$, $\nu_s=0.34$; Layer 2 is titanium with $E_{ti}=1.05\ 10^{11}\ Pa$, $\nu_{ti}=0.29$.

The objective of this application is to identify the indentation area and the pressure distribution anywhere on the solid boundaries by using the overspecified data measured on Γ_m. The measured data are generated numerically by solving the direct problem where the pressurized area (disk with radius R_p) and the expression of the pressure distribution as a function of the radius r are given:

$$p=\frac{-8\mu\sqrt{(R_p^2-r^2)}}{1+x_i} \quad with \quad x_i=\frac{\lambda+3\mu}{\lambda+\mu},\ \lambda=\frac{\nu_s E_s}{(1-2\nu_s)(1+\nu_s)},\ \mu=\frac{E_s}{2(1+\nu_s)} \tag{56}$$

The direct and inverse problems have been carried out using Comsol software [17].

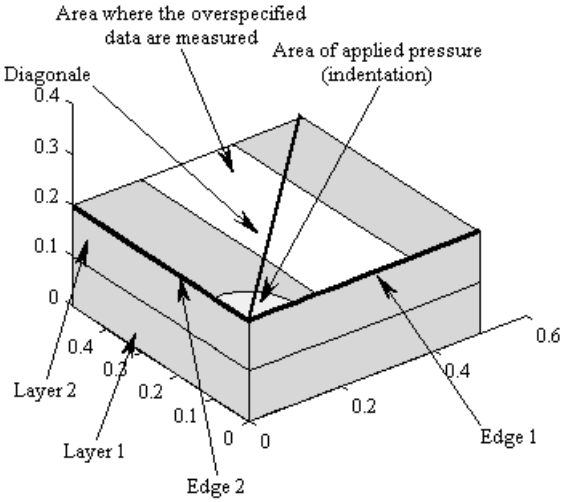

Fig. 5. The geometry of the solid.

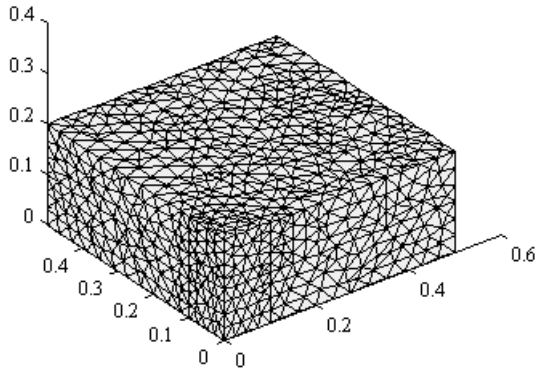

Fig. 6. The mesh of the solid.

Figures 5 and 6 display the geometry and mesh used in this study. The number of nodes on Γ_u is *345*, whereas the number of nodes on Γ_m is *134*. Hence, there are *345x6=2070* variables for the optimization problem for only *134x6=804* overspecified known data. The mesh must be regular and sufficiently refined. However, an excessive mesh refinement leads to a very poorly conditioned Hessian of the error function with a reduced convergence rate and possible oscillations in the solution.

Figures 7 to 30 show various fields obtained by the exact and the identified solutions. Figures 7 and 8 show the map of the displacement norm $\|u\|$ obtained from the exact and the identified solutions. Figures 9 and 10 show the map of the Von Mises equivalent stress obtained from the exact and the identified solutions. Figures 11 to 16 show the profiles of the displacement component u_z, the Von Mises equivalent stress σ_{eq} and the stress component σ_{zz} on edges 1 and 2 and on the diagonal line, as shown on Figure 5. Good correlations between the exact and identified fields can be observed.

The identified solutions depend on the quality of the measured data. Here, the measured data are extracted from finite element results of the direct indentation problem. The exact indentation pressure has a parabolic profile as shown in figures 15 and 16 (exact pressure). However, the distributed indentation pressure used in the direct problem depends on the refinement of the mesh as shown in figures 15 and 16 (σ_{zz}^{e}). Hence, the measured data (Neumann and Dirichlet) issued from that direct problem is altered with a level noise that is a function of the mesh refinement. Then, the identified pressures are also altered with the same noise and as shown on figures 15 and 16, (σ_{zz}^{I}).

Figures 17 and 18 map the exact and identified displacement normal component u_z and Von Mises equivalent stress distributions on a diagonal section of the solid. These show good agreement with the exact fields for the displacement component u_z and Von Mises equivalent stress. The stress discontinuity at the interface of the two materials is well recovered. Figures 21 to 26 show maps of the exact and identified displacement component u_z, the stress component σ_{zz} and the norm of the tangential stress vector σ_t defined by equation (57) below, distributed on the top face of the solid. Here, too, a good correlation exists between the exact and identified results.

$$\sigma_t = \sqrt{\sigma_{xz}^2 + \sigma_{yz}^2} \tag{57}$$

Figures 27 to 30 show the maps of the exact and identified stress component $-\sigma_{zz}$ and the norm of the tangential stress vector σ_t, distributed on the interface between the two materials of the solid. Here, too, a good correlation exists between the exact and identified results with reasonable accuracy, even for the interface tangential stress.

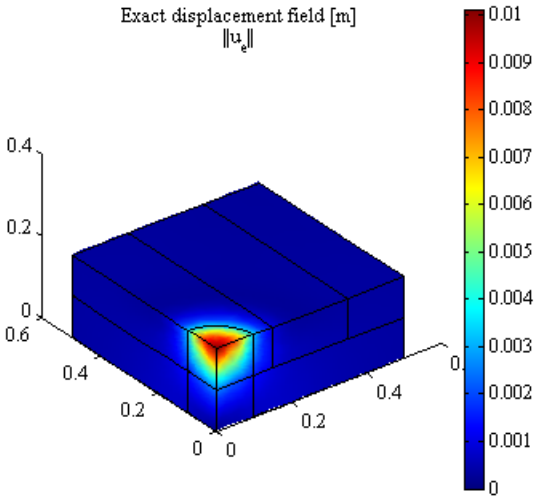

Fig. 7. Exact displacement field.

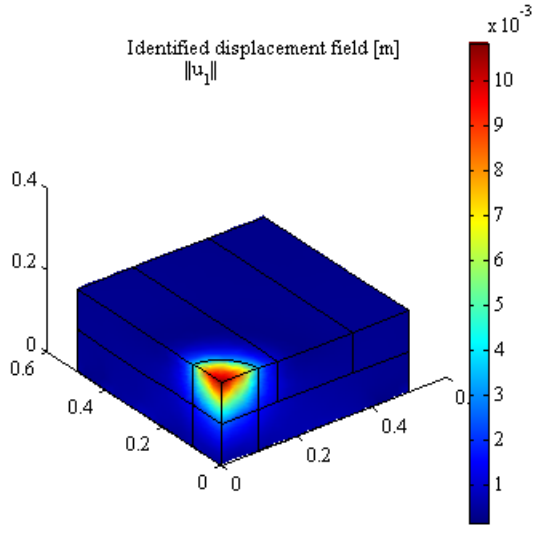

Fig. 8. Identified displacement field

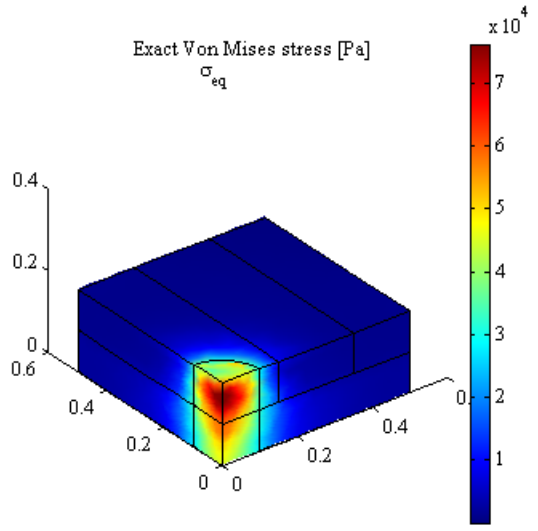

Fig. 9. Exact Von Mises equivalent stress.

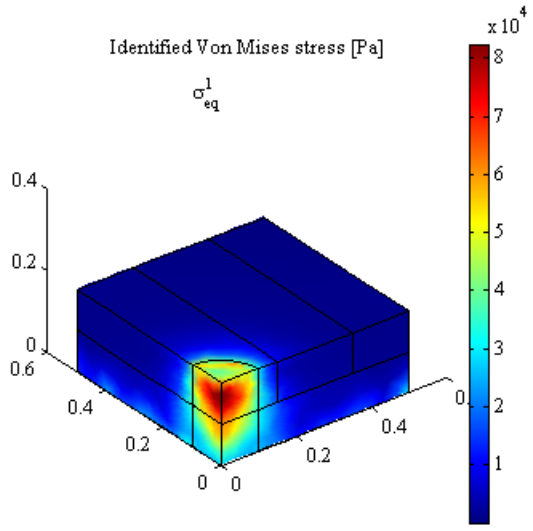

Fig. 10. Identified Von Mises equivalent stress

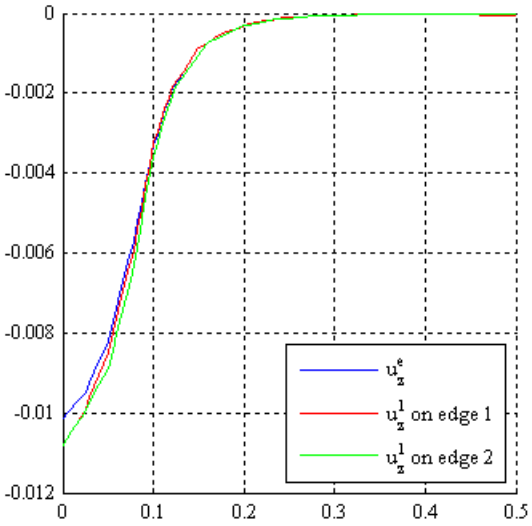

Fig. 11. Exact and identified displacement u_z on the edges

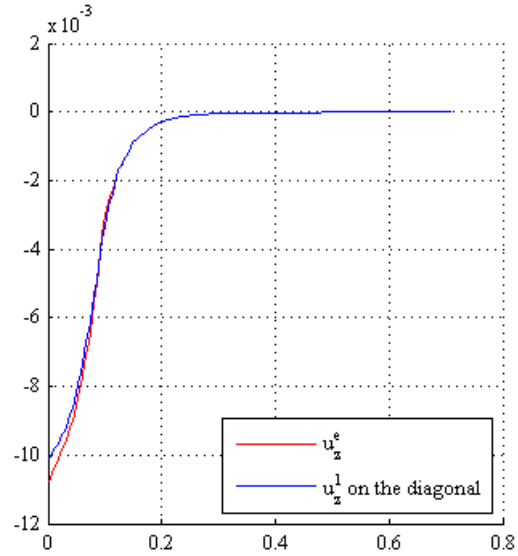

Fig. 12. Exact and identified displacement u_z on the diagonal line

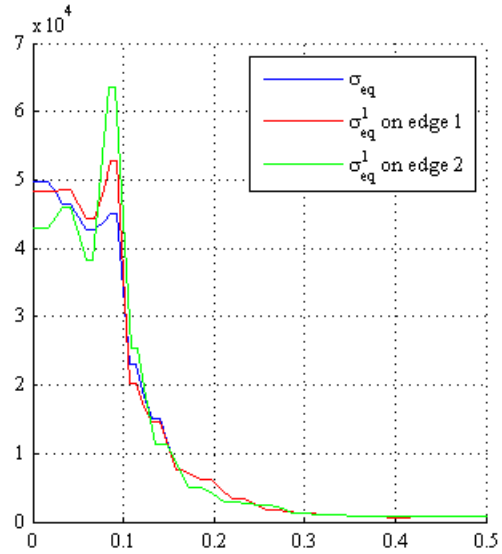

Fig. 13. Exact and identified Von Mises equivalent stress σ_{eq} on the edges

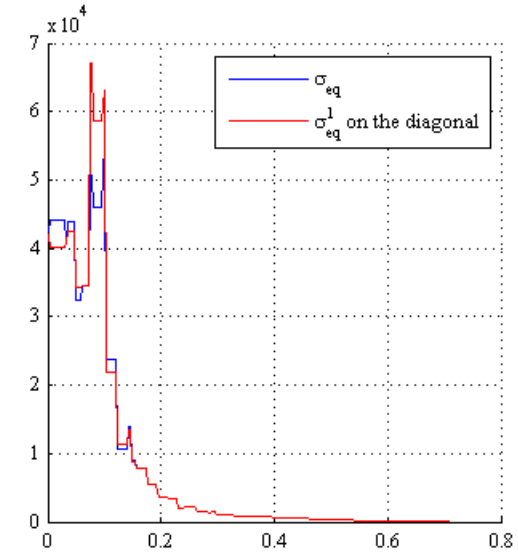

Fig. 14. Exact and identified Von Mises equivalent stress σ_{eq} on the diagonal line

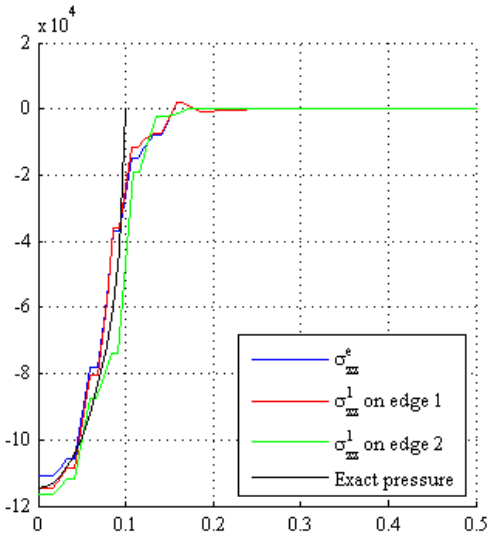

Fig. 15. Exact and identified stress σ_{zz} on the edges

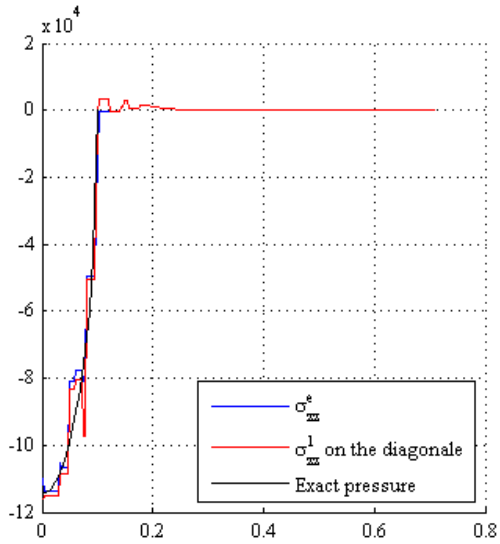

Fig. 16. Exact and identified stress σ_{zz} on the diagonal line

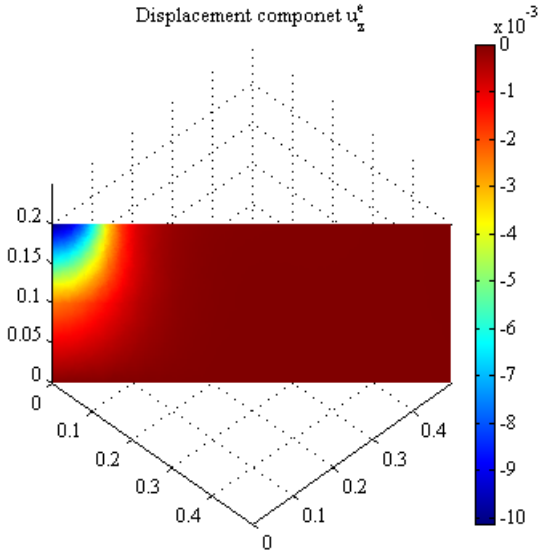

Fig. 17. Exact displacement u_z on the diagonal section.

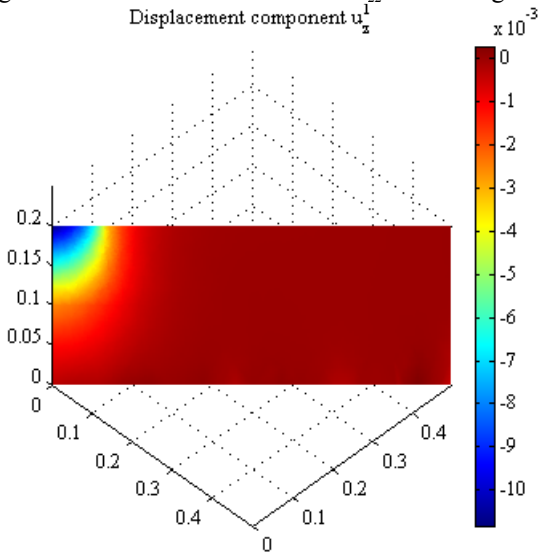

Fig. 18. Identified displacement u_z on the diagonal section.

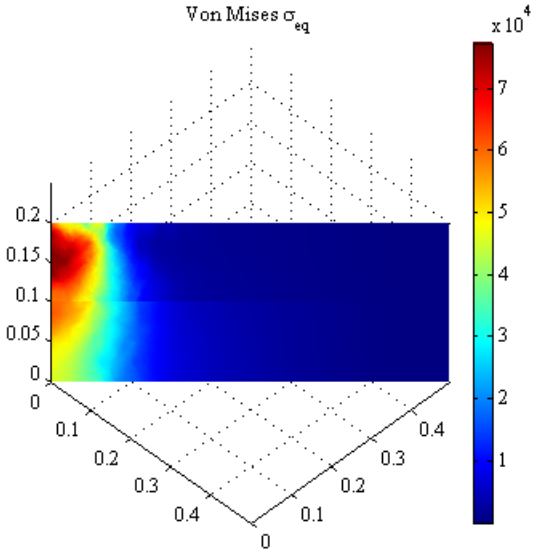

Fig. 19. Exact Von Mises equivalent stress on the diagonal section.

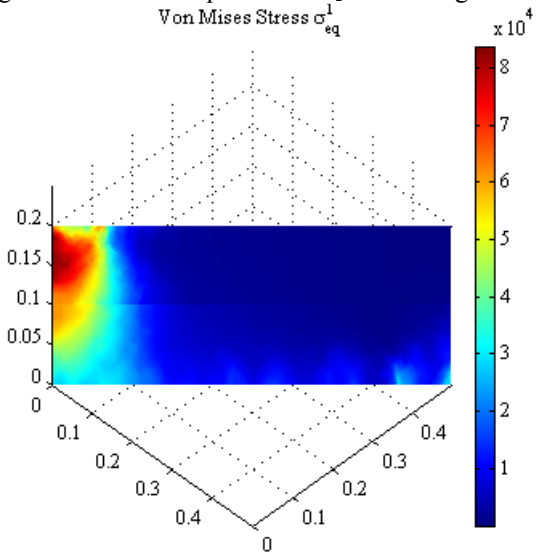

Fig. 20. Identified Von Mises equivalent stress on the diagonal section

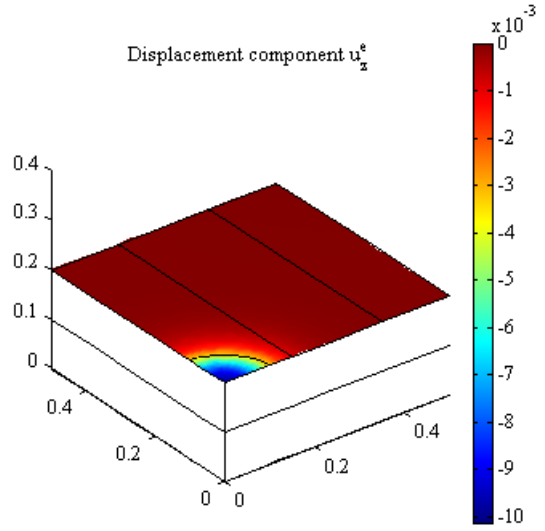

Fig. 21. Exact displacement u_z on the top face.

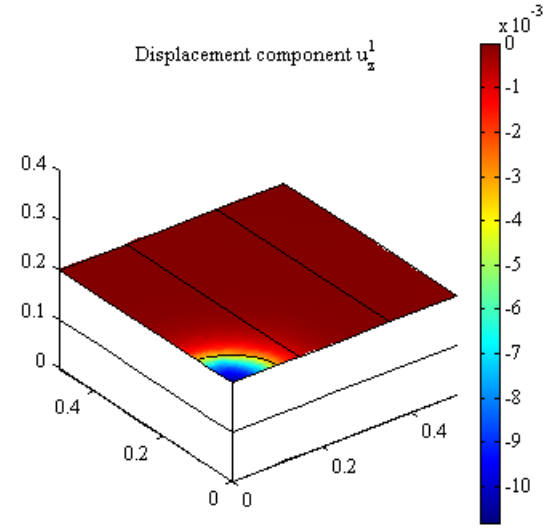

Fig. 22. Identified displacement u_z on the top face.

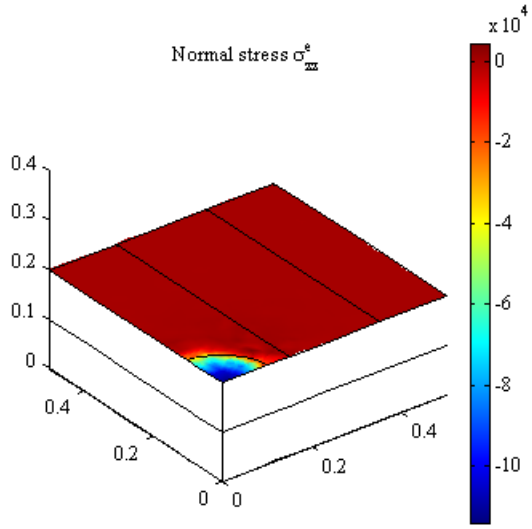

Fig. 23. Exact stress σ_{zz} on the top face.

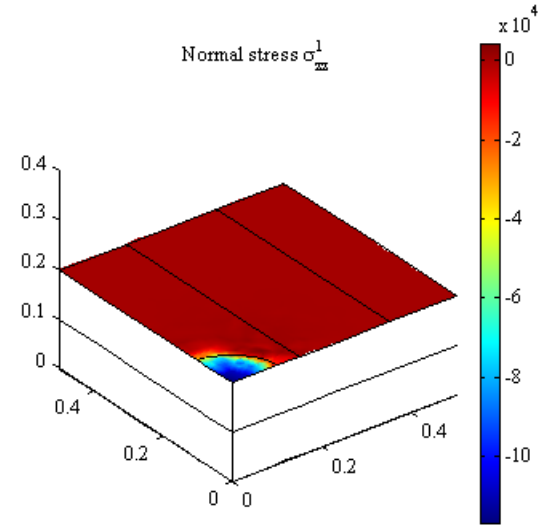

Fig. 24. Identified stress σ_{zz} on the top face

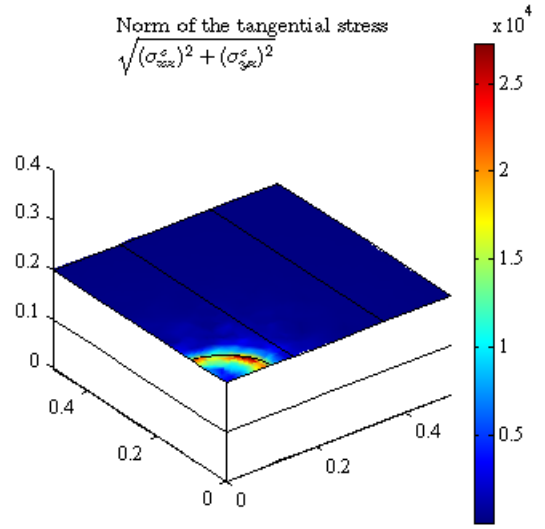

Fig. 25. Exact tangential stress on the top face.

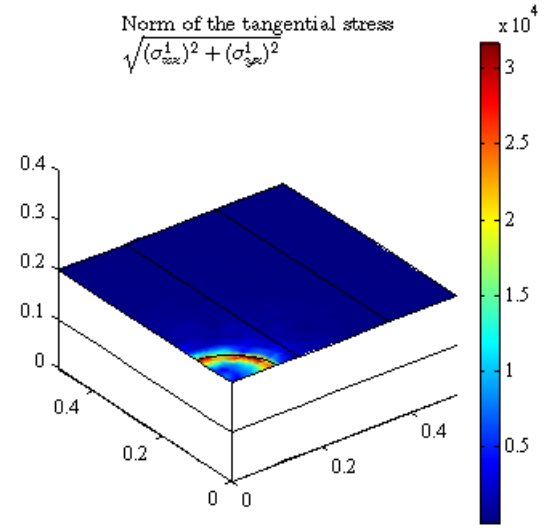

Fig. 26. Identified tangential stress on the top face

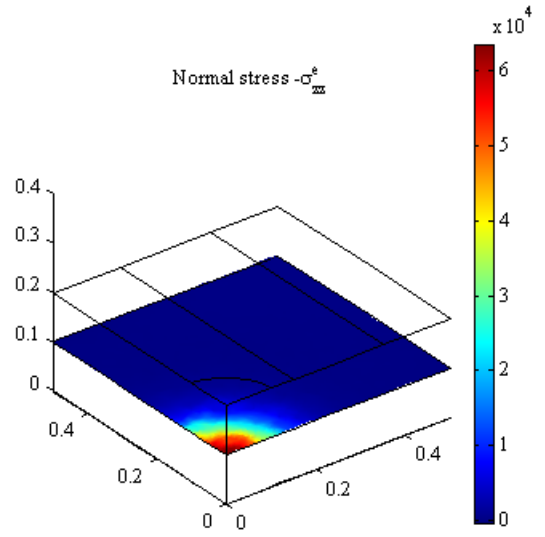

Fig. 27. Exact stress -σ_{zz} on the interface.

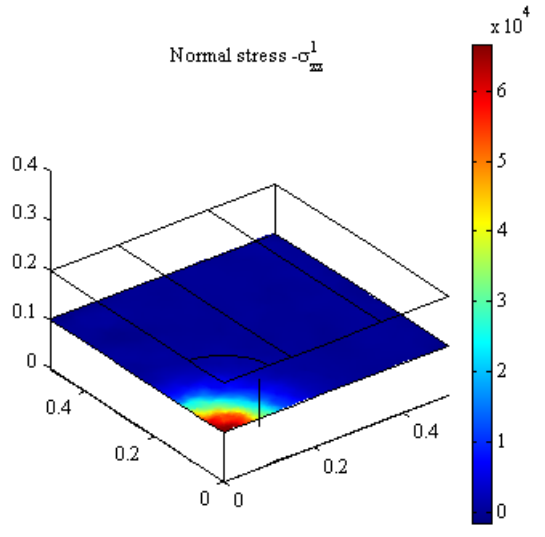

Fig 28. Identified stress -σ_{zz} on the interface.

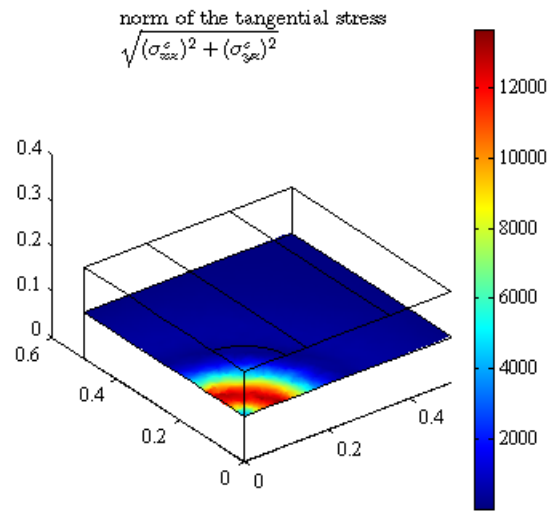

Fig. 29. Exact tangential stress on the interface.

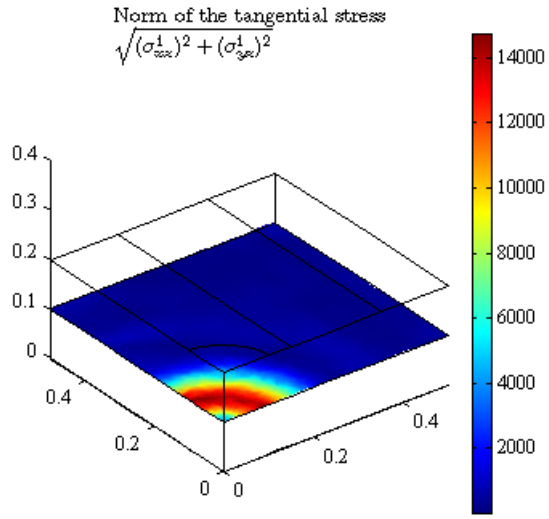

Fig. 30. Identified tangential stress on the interface.

8.2 Contact areas identification of three-dimensional solids.

As mentioned before, the boundary conditions on parts Γ_m and Γ_u of the solid boundary can be non-linear, as when they involve contact and friction. This application considers two solids with different contact areas induced by external loads. The problem has two planes of symmetry. Hence, only one quarter is modeled. Figure 31 shows the deformed shape and the distribution of the displacement field issued from the direct problem, defined as follows:

- ✓ The first solid is a cylinder with radius r=*0.248 m* and a length *L=3 m*. The material is steel with a Young's Modulus $E=2.1\ 10^{11}$ Pa and a Poisson coefficient $\nu=0.34$.
- ✓ The second solid is a rectangular box of dimension *1x1x2 m*, which contains a cylindrical hole of radius *0.250 m*. The material is aluminum with a Young's Modulus $E=7\ 10^{10}$ Pa and a Poisson coefficient $\nu=0.27$.
- ✓ The face *y=0* is clamped: $u = v = w = 0$.
- ✓ The face *x=0* is a plane of symmetry and is fixed in the *x* direction: $u=0$.
- ✓ The face *z=0* is a plane of symmetry and is fixed in the *z* direction: $w=0$.
- ✓ On the circular face of the cylinder at *z=1.5 m*, a displacement is prescribed in the y direction: $D_{imp}=-0.1\ m$.
- ✓ Initially, the two solids have no contact.

A static nonlinear finite element analysis was carried out using finite elements with the Code-Aster [16]. The result is displayed in figure 27. Two contact areas between the solids are highlighted. From this analysis, *measured data* (displacements and forces) are extracted on Γ_m for use in the identification problem, which is carried out using Comsol software [17]. Figure 28 shows the geometry used in the identification problem: the cylinder is ignored. The *measured data* extracted from the above direct problem are applied on Γ_m. The mesh used in this case has *2646* nodes, *4200* elements, *315* nodes on Γ_u and *336* nodes on Γ_m. The identification necessitates 16 trust region iterations.

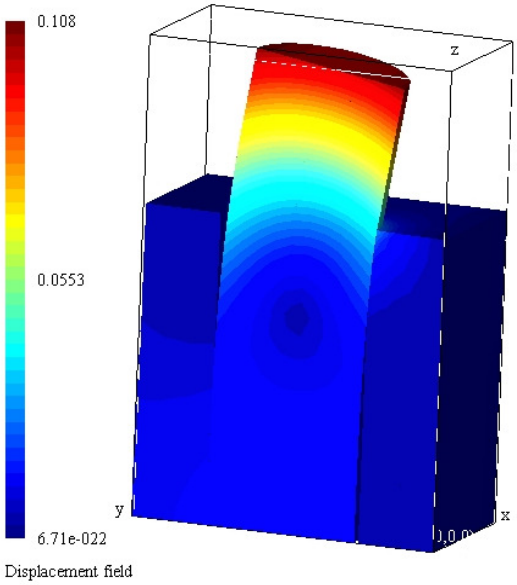

Fig. 31. Displacement field distribution in the direct problem

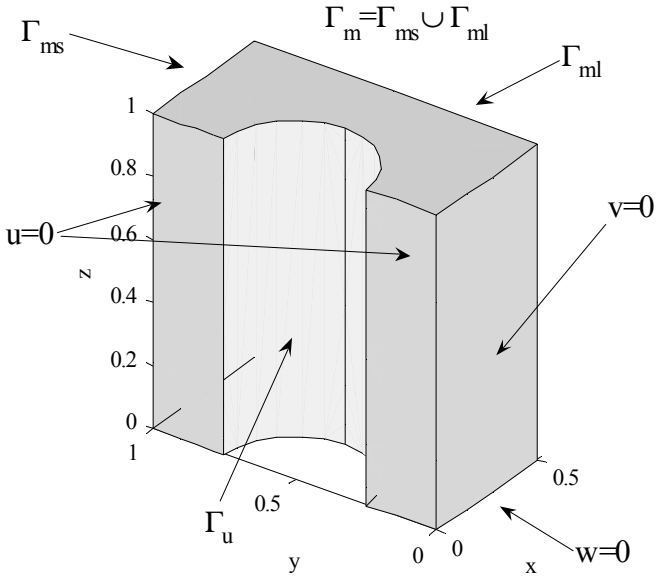

Fig. 32. The geometry used in the identification process.

Figures 33 and 34 show the maps of the exact displacement fields and normal stress component $\sigma.n.n$ distributed on the surface Γ_u. Figures 35 and 36 show the maps of the identified displacement fields and normal stress component $\sigma.n.n$ distributed on the surface Γ_u. In the case where all measured data are used (three displacements and three forces components), the identification is in good agreement with the exact results.

Figures 37 and 38 show the maps of the exact displacement fields and normal stress component $\sigma.n.n$ distributed on the surface Γ_u. In this case, incomplete data are used (Incomplete Cauchy problem): only tangential displacements on Γ_m are used for the identification problem, the normal displacement is left unknown. The identification necessitates 26 trust region iterations. Even though, as expected, a slight degradation of the result is observed, the contact areas and pressure distributions can be still identified with reasonable accuracy.

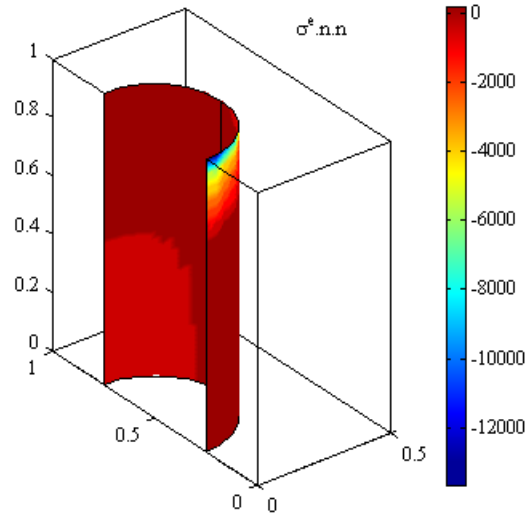

Fig. 33. Exact normal stress $(\sigma n).n$.

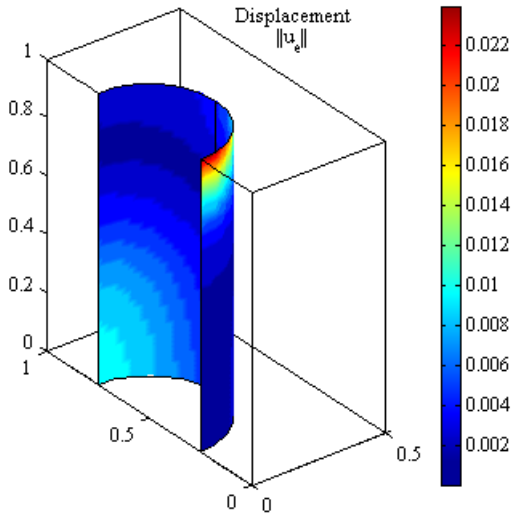

Fig. 34. Exact displacement field

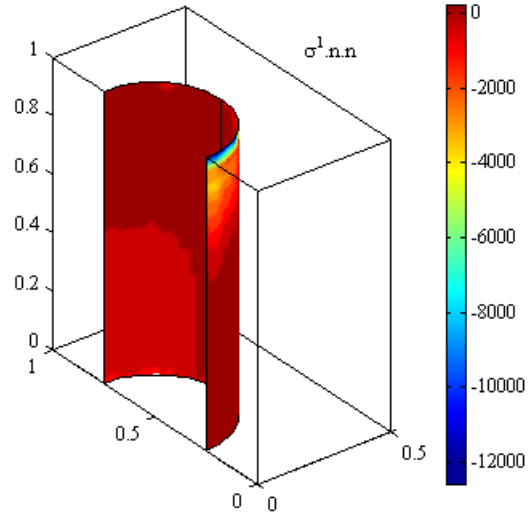

Fig. 35. Identified normal stress $(\sigma n).n$.

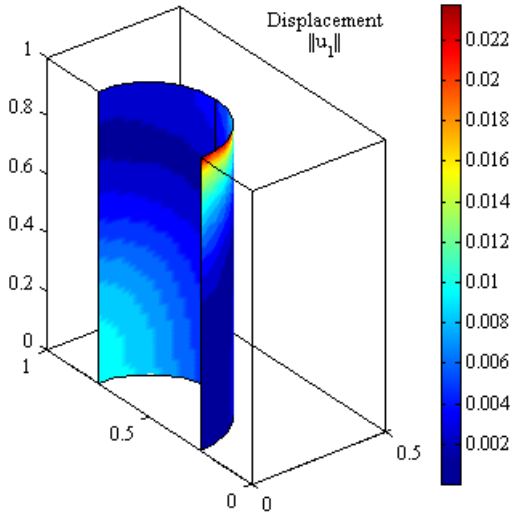

Fig. 36. Identified displacement field.

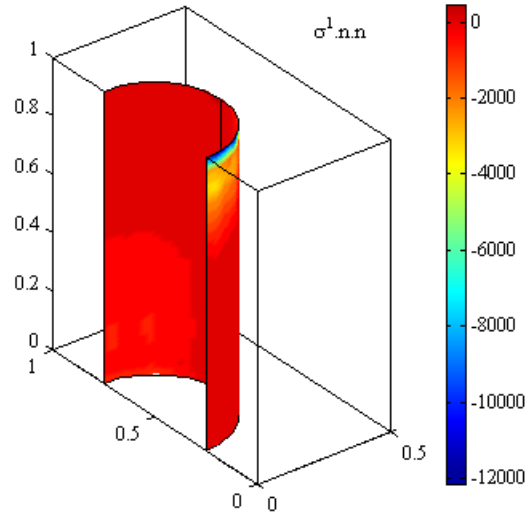

Fig. 37. Identified normal stress $(\sigma n).n$ obtained with incomplete data

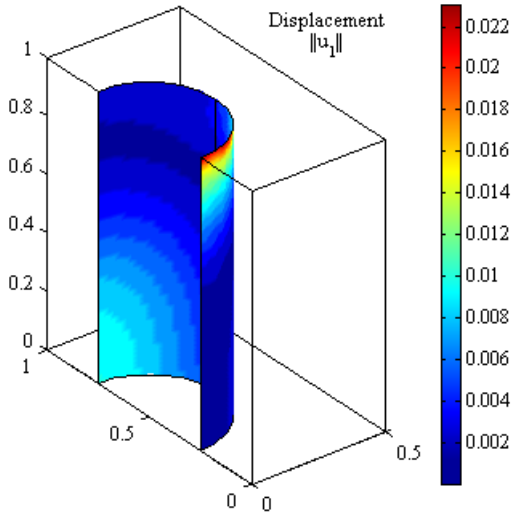

Fig. 38. Identified displacements field obtained with incomplete data.

8.3 Comparison with Kozlov–Maz'ya–Fomin's algorithm.

The following table shows the performance of the two procedures for solving the Cauchy problem. The first one is the energy error minimization method, whereas the second one is the alternating KMF algorithm described in part 6. The KMF algorithm is stopped when the value of the energy function reaches that obtained by the trust region method. Clearly, the trust region method performs far better, as anticipated in part 6.

Application	Trust Region Method For energy error minimization	KMF Method
Identification of indented area	185	23 000
Identification of contact area with complete data	16	40 000
Identification of contact area with incomplete data	26	50 000

Table 1. Number of iterations needed by each algorithm for convergence.

8.4 Sensitivity to the amount and localisation of measured data.

Contrary to the framework of the continuous medium where the size of Γ_m does not play any role in the existence and uniqueness result for the solution of the Cauchy problem, in the discretized domain and according to the applications treated in this paper it appears that the identified data are as well sensitive to the quantity of overspecified data as to their localization. However, the amount of the overspecified data should not necessarily be equal to or higher than that of the data to identify: the ratio of the amount overspecified data on the unknown ones is not the essential parameter. A judicious choice of both the amount of measurements and their localization must be carried out according to the available information concerning the data to be identified. We made the following experiment by considering the second application relating to the identification of contact zone. The boundary Γ_m in figure 32 is subdivided in two sub-boundaries such that $\Gamma_m = \Gamma_{ms} \cup \Gamma_{ml}$. Where Γ_{ms} denote the top face of Γ_m, and Γ_{ml} the lateral side of Γ_m. Using the same mesh above, two cases are studied:

- ✓ Case 1: overspecified data are defined on Γ_{ms}. We have 126 nodes on Γ_{ms} and 315 nodes on Γ_u.
- ✓ Case 2: overspecified data are defined on Γ_{ml}. We have 231 nodes on Γ_{ml} and 315 nodes on Γ_u.

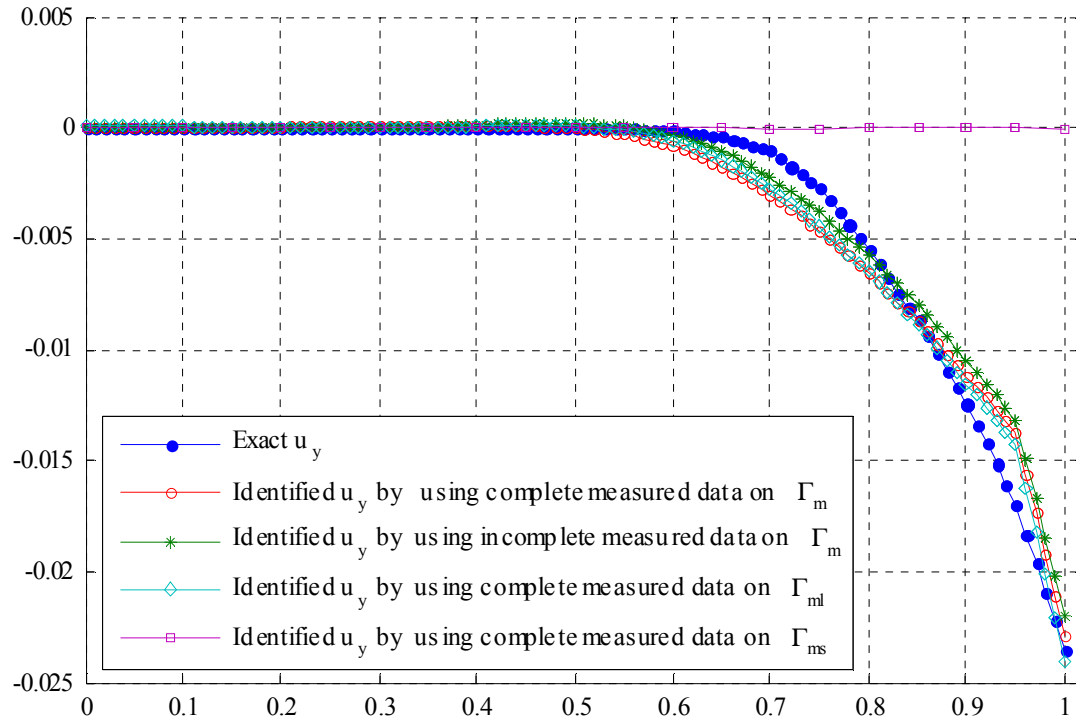

Fig. 39. Sensitivity of the identified displacement u_y along the edge x=0 and y=0.25, to the amount and localization of the overspecified data.

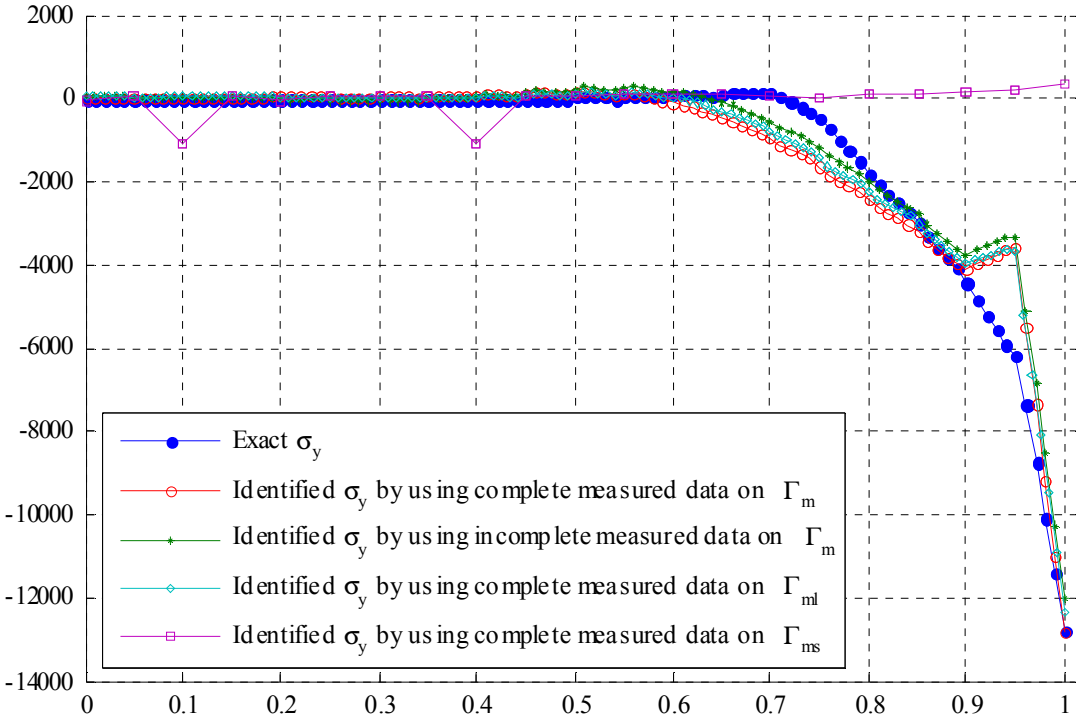

Fig. 40. Sensitivity of the identified stress σ_y along the edge x=0 and y=0.25, to the amount and localization of the overspecified data.

The figures 39 and 40 show the identified displacement u_y and stress $\sigma_{y\,y}$ along the edge defined by $x=0$ and $y=0.25$. Note that the mesh is not particularly refined (the size of the element side is 0.5). We can see that the identified data obtained by using complete and incomplete data on Γ_m are very close to those obtained by using complete data on Γ_{ml}. However, when the overspecified data are only defined on Γ_{ms}, the identified data are very bad and unusable. In this situation, few overspecified data are used and simultaneously a very low sensitivity of the displacement on the Γ_{ms} part with respect to surfaces traction applied along the edge ($x=0$ and $y=0.25$) of the solid has to be expected. The two cases presented are extreme; other cases not described here shows that it is possible to obtain good results with an optimized amount and localization measurements as soon as a the location of the measurement is chosen so as to exhibit a reasonable sensitivity with respect to displacement and surface traction on the unreachable part of the boundary.

9 Conclusion

A general method has been developed in this paper to solve Cauchy problems in elasticity and consequently to identify boundary conditions. This method is based on the idea of exploiting simultaneously and symmetrically the overspecified data measured on the accessible boundary. Next, two well-posed problems are defined. The first one involves the unknown Neumann boundary condition and the measured Dirichlet boundary condition. The second one involves the unknown Dirichlet boundary condition and the measured Neumann boundary condition. The two problems can also have additional usual boundary conditions. An energy error functional is then designed to measure the gap between the solutions of these two problems. This functional is positive and cancels when the difference between the two fields reduces to a rigid body displacement field. An optimization approach is then used to minimize this functional, which depends explicitly on the above fields and implicitly on the unknown boundary conditions. The optimization is carried out using the Trust Region Method, which has good regularizing properties and an adjoint field method for the computation of the gradients. The convergence is achieved with far fewer iterations in comparison to the well-known method of Kozlov *et al.* [28].

Two examples have been presented. The first deals with the indentation of a bi-layered solid. The results obtained are in good agreement with the exact ones, even if the area of the measured data is smaller than the area where the data are identified. The second example addresses the identification of three-dimensional contact areas. In this case, the boundary conditions to be identified are non-linear. In spite of this non-linearity, the results are in good agreement with those obtained by the exact solution. The same example is also solved with incomplete data. Only tangential displacement components are used, the normal components being unknown. In this case, in spite of the loss of accuracy, the identification of contact areas remains possible. These last results confirm the possibility of using the method in conjunction with image correlation tools that deliver only tangential information on surface displacements or strain fields. Once the boundary data are computed, some additional identification techniques can be used in order to gain information about the physical parameters entering into the non-linear boundary condition on Γ_u if its nature is known, as in the case of the friction coefficient. This will be a subject of forthcoming paper.

The presented method can be easily implemented in industrial finite element software in order to deal with industrial identification problems. No regularization is needed. However, in the case of industrial applications, the data are often severely altered by noise. Hence, the identification will also be altered by this noise. The effect of noise has been examined for the Cauchy problem for the Laplacian operator in a previous paper of Andrieux *et. al*. [3]; incorporation of some kind of regularization seems to be requisite in the method as soon as the noise is above 5%.

References

[1] Allix O. and Feissel P., 2003, A delay-damage meso-modeling of laminates under dynamic conditions : basic aspects and identification issues, Computers and Structures, 81 (12), 1177-1191.

[2] Andrieux S., Ben Abda A. and Baranger T.N., 2005, Data completion via an energy error functional, C. R. Mécanique, 333, 171-177

[3] Andrieux S., Baranger T.N. and Ben Abda A., 2006, Solving Cauchy problem by minimizing an energy-like functional, Inverse Problems 22, 115-133.

[4] Ang D.D., Ikehata M. and Trong D.D, 1998, Yamamoto M., Unique continuation for a stationary isotropic Lamé system with variable coefficients, Comm. Part. Diff. Eq, 23, 371-385.

[5] Bakushinsky A B and Kokurin M Yu, 2004. Iterative Methods for Approximate Solution of Inverse Problems (Dordrecht: Springer).

[6] Baumeister J., Leitão, A., 2001, On iterative methods for solving ill-posed problems modelled by partial differential equations, J. of Inverse and Ill-posed problems, 9, 13-30.

[7] Bernstsson F. and Elden L., 2001, Numerical solution of a Cauchy problem for the Laplace equation, Inverse Problems, 17, 839-853.

[8] Bonnet M. and Constantinescu A., 2005, Inverse problems in elasticity, Inverse Problems 21 R1-R50.

[9] Bourgeois L., 2005, A mixed formulation of quasi-reversibility to solve the Cauchy problem for the Laplace equation, Inverse Problems, 21, 1087-1104.

[10] Bui H.D., 1996, Inverse problems in the mechanics of materials: an introduction. CRC Press, Boca Raton, USA.

[11] Bui H.D., 1986, Transformation des données aux limites relatives au demi-plan élastique homogène et isotrope, Int. J. Solids Structures, Vol. 4,1025-1030.

[12] Brian H.D., Dulikravich G. and Yoshimura S. A, 2004, Finite element formulation for the determination of unknown boundary conditions for three dimensional steady thermo-elastic problems., J. Heat Transfer, ASME, Vol.126, 110-118.

[13] Brown B. M., Jais M. and Knowles I. W. 2005, A variational approach to an elastic inverse problem, Inverse Problems, 21, 1953-1973.

[14] Byrd, R.H., Schnabel R.B., and Shultz G.A. 1988, Approximate Solution of the Trust Region Problem by Minimization over Two-Dimensional Subspaces, Mathematical Programming, Vol. 40, 247-263.

[15] Cimetière A., Delvare F., M. Jaoua M. and F. Pons, 2001, Solution of the Cauchy problem using iterated Tikhonov regularisation, Inverse Problems, 17, 553-570.

[16] Chavent G., 1991, On the theory and practice of non-linear least squares. Advances in Water Resources, 14(2), 55-63.

[17] Chouaki A, Ladevèze P and Proslier L, 1996, An updating of structural dynamic model with damping *Inverse Problems in Engineering: Theory and Practice* ed D Delaunay, M Raynaud and K Woodbury (New York: ASME) pp 335–42

[18] Code-Aster, 2007, EDF, Clamart, France. www.Code-Aster.org.

[19] Comsol, 2007, Comsol Multiphysics. www.comsol.fr.

[20] Coleman T. F. and Li Y., 1996, An interior trust region approach for nonlinear minimization subject to bounds, SIAM J. Optim., 6, 418–45.

[21] Constantinescu A., 1995, On the identification of elastic moduli from displacement-force boundary measurements, Inverse problems in Engrg., 1, 293-315.

[22] Dehman B. and Robbiano L., 1993, La propriété du prolongement unique pour un système elliptique : le système de Lamé, J. Math. Pures et Appliquées, 72, 475-492.

[23] Delvare F. and Hanus J.L., 2005, Complétion de données par méthode inverse en élasticité linéaire, 7eme Colloque National en Calcul de Structures, 17-20 mai 2005, Giens, France.

[24] Deraemaeker A, Ladevèze P and Leconte Ph 2002 Reduced bases for model updating in structural dynamics based on constitutive relation error *Comput. Methods. Appl. Mech. Eng.* **191** 2427–44

[25] Fursikov A., 2000, Optimal Control of Distributed Systems-Theory and Applications, Translations of Math. Monographs, Vol. 187, American Mathematical Society, Providence, RI, USA.

[26] Geymonat G., Hild F., Pagano S., 2002, Identification of elastic parameters by displacement field measurement, C.R. Mécanique, 330, 403-408.

[27] Griewank A.,1993, Some bounds on the complexity of gradients, jacobians, and hessians. Technical Report MCS-P355-0393, Mathematics and Computer Science Division, Argonne National Laboratory.

[28] Hadj-Sassi K., Andrieux S., 2006, Parameter identification of a non linear viscoelastic model via an energy error functionnal, ECCM 6, Lisbonne, july 2006.

[29] Hon Y.C. and Wei T., 2001, Backus-Gilbert algorithm for the Cauchy problem of the Laplace equation, Inverse problems, 17, 261-271.

[30] Kohn R.V. and Mc Kenney A., 1990, Numerical implementation of a variational method for electric impedance tomography, Inverse Problems, 6, 389-414.

[31] Kokurin M. Y., 2006, Stable iteratively regularized gradient method for nonlinear irregular equations under large noise, Inverse Problems 22, 197-207.

[32] Kozlov V.A., Maz'ya V.G., Fomin A.V., 1991, An iterative method for solving the Cauchy problem for elliptic equations, Comput. Meth. Math. Phys., Vol. 31, N°1, 45-52.

[33] Kozlov V., Maz'ya V., Fomin A., 1994, The inverse problem of coupled thermo-elasticity, Inverse Problems, 10, 153-160.

[34] Ladevèze P and Chouaki A 1999 Application of *a posteriori* error estimation for structural model updating, *Inverse Problems* **15** 49–58

[35] Ladevèze P and Leguillon D 1983 Error estimates procedures in the finite element method and applications, *SIAM J. Numer. Anal.* **20** 485–509

[36] Ladevèze P., Reynier M. and Maia N.M., 1994, Error on the constitutive relation in dynamics: theory and applications for model updating. ISIP 94 : Second international symposium on Inverse problems in engineering Mechanics. Paris, 2-4 Nov, H.D. Bui and M.Tanaka eds, Balkema, Rotterdam, 251-256.

[37] Marin L. and Lesnic D., 2004, The method of fundamental solutions for the Cauchy problem in two-dimensional linear elasticity, International Journal of Solids and Structures, 41, 3425-3438.

[38] Marin L. and Lesnic D., 2002, Boundary element solution for the Cauchy problem in linear elasticity using singular value decomposition, Comp. Meth. App. Mech. Eng., 29-30, 2002, 3257-3270.

[39] Matlab Software Copyright 1984–2000 The MathWorks, Inc.

[40] Rota L., 1994, An inverse approach for identification of dynamic constitutive equations. ISIP 94: Second international symposium on Inverse problems in engineering Mechanics. Paris, 2-4 Nov 1994, H.D. Bui and M.Tanaka eds, Balkema, Rotterdam, 251-256.

[41] Sutton M.A., Cheng M., Peters W.H., Chao Y.S., McNeill S.R., 1986, Application of an optimized digital correlation method to planar deformation analysis, Image vision Computing, 4 (3), 143-150.

[42] Tikhonov A. N. and Arsenin V. Y., 1977, Solution to Ill-posed Problems, New York: Winston-Wiley.